

Reconstructing Sea Surface Salinity in the Labrador Sea

Joseph Lawson
24914231

MSci Oceanography
2014 – 2015

School of Ocean and Earth Science
University of Southampton

Advanced Independent Research Project (6071)
Project Supervisor: **Dr Eleanor Frajka-Williams**

Word Count: 9768

Abstract

Salinity in the Labrador Sea is an important factor in convection and deep water formation as it dominates physical water column structure. As a major location for deep water formation the Labrador Sea is sensitive to additions of freshwater, as it acts to stabilise seawater in the buoyancy budget (Solomon *et al*, 2007). Based on surface layers of the Labrador Sea tending to be both fresh and cold, the motivation for this study was to understand salinity influences by generating a Sea Surface Salinity (SSS) lookup table between 50°N, 65°W – 65°N, 45°W to estimate SSS from Sea Surface Temperature (SST). The data used to construct temperature - salinity relations for the lookup table was Argo float data between 50°N, 65°W – 65°N, 45°W from January 2002 - December 2012. UK Met Office OSTIA SST data from August 2011 - February 2015 was used to reconstruct SSS and National Aeronautics and Space Administration (NASA) derived Aquarius SSS data from August 2011 - February 2015 was used to compare reconstructed SSS against, both between 50°N, 65°W – 65°N, 45°W. Results show a tight Argo temperature - salinity relationship exists in winter months, allowing SSS to be reconstructed reasonably accurately. In contrast summer temperature - salinity relations ‘breakdown’, proving problematic to reconstructing salinity from temperature. Reconstructed SSS correlates reasonably with Aquarius in the East and West Basin but not in the central basin, although further analysis and research is undoubtedly required. Salinity is relatively under-sampled in sub-polar oceans and low in resolution, making the ability of estimate salinity from existing data a simple and cost effective solution. The possibilities of such a look up table are an exciting prospect and potential applications broad, ranging from vertical reconstruction of salinity, density and velocity, to a better understanding of freshening influences on the AMOC and identification of deep convection.

Acknowledgments

I would like to thank Dr. Eleanor Frajka-Williams for support and guidance throughout this project. Additional thanks go to Lena Schulze for pre-processing and use of her December 2002 – December 2012 Argo Float dataset.

Table of Contents

1	Introduction.....	4
1.1	General Introduction to the Labrador Sea	4
1.2	Significance of Salinity	4
1.3	New Era of Data	5
1.4	Study Research Aims.....	6
2	Background.....	6
3	Data.....	7
3.1	Argo Floats	7
3.2	Combined Satellite and In-situ SST	8
3.3	Satellite SSS	9
4	Variability of Surface Temperature and Salinity from Argo	10
4.1	Argo Float Surface Representation.....	10
4.2	Temporal Variability and Long Term Trends	13
5	Monthly Temperature-Salinity Relationship	18
6	Quantifying the surface T-S relationship.....	22
6.1	Upper and Lower Bounds.....	22
6.2	Methods for T-S Transfer Relationship.....	24
6.2.1	Linear Regression	25
6.2.2	Quadratic Regression.....	28
6.2.3	Mixed Effects Spline Regression.....	31
7	Evaluating Regression Choice	34
7.1	Temperature Averaged Salinity Residuals	34
7.2	Temperature Averaged Salinity Root Mean Squared.....	37
8	SSS Reconstructions	40
9	SSS Reconstructions Compared to Aquarius.....	45
10	Discussion.....	48
10.1	Limitations.....	50
10.2	Potential Application	52
11	Conclusion	52
11.1	Summary of Results	52
11.2	Future Considerations.....	53
11.3	Take Home Message	53
12	References.....	54

Figure Table of Contents

Figure 1 January 2002 - December 2012 Argo float temperature measurements shallower than 10m vs nearest OSTIA level 4 SST	10
Figure 2 January 2002 - December 2012 Argo float temperature measurements shallower than 5m vs nearest OSTIA level 4 SST	10
Figure 3 January 2002 - December 2012 Argo float temperature measurements shallower than 10m with Argo profiles removed vs nearest OSTIA level 4 SST	11
Figure 4 January 2002 - December 2012 Argo float temperature measurements shallower than 5m with Argo profiles removed vs nearest OSTIA level 4 SST	11
Figure 5 January 2002 - December 2012 Argo profile locations shallower than 10m (post Argo profile removal)	13
Figure 6 Box and whisker diagrams of temperature and salinity of classified Shelf, West Basin and East Basin regions	14
Figure 7 January 2002 - December 2012 time series of East and West Basin Argo float temperature collected shallower than 10m	15
Figure 8 January 2002 - December 2012 time series of East and West Basin Argo float salinity collected shallower than 10m	15
Figure 9 West Basin Argo float profile locations and corresponding salinity during summer months (December, January, February and March) of 2005	16
Figure 10 West Basin Argo float profile locations and corresponding salinity during summer months (December, January, February and March) of 2008	16
Figure 11 West Basin Argo float shallower than 10m temperature and salinity monthly diagrams overlaid onto seawater density contours	18
Figure 12 East Basin Argo float shallower than 10m temperature and salinity monthly diagrams overlaid onto seawater density contours	19
Figure 13 West Basin Argo float shallower than 10m temperature and salinity monthly diagrams overlaid onto seawater density contours	22
Figure 14 East Basin Argo float shallower than 10m temperature and salinity monthly diagrams overlaid onto seawater density contours	23
Figure 15 West Basin Argo float shallower than 10m temperature and salinity monthly diagrams overlaid onto seawater density contours	25
Figure 16 East Basin Argo float shallower than 10m temperature and salinity monthly diagrams overlaid onto seawater density contours	26
Figure 17 West Basin Argo float shallower than 10m temperature and salinity monthly diagrams overlaid onto density contours	28
Figure 18 East Basin Argo float shallower than 10m temperature and salinity monthly diagrams overlaid onto density contours	29
Figure 19 West Basin Argo float shallower than 10m temperature and salinity monthly diagrams overlaid onto density contours	31
Figure 20 East Basin Argo float shallower than 10m temperature and salinity monthly diagrams overlaid onto density contours	32
Figure 21 West Basin Argo float salinity shallower than 10m vs salinity residuals of piecewise linear, quadratic and mixed effect spline regression methods	34
Figure 22 East Basin Argo float salinity shallower than 10m vs salinity residuals of piecewise linear, quadratic and mixed effect spline regression methods	35
Figure 23 West Basin Argo float salinity shallower than 10m vs salinity root mean squared (RMS) of piecewise linear, quadratic and mixed effect spline regression methods	37
Figure 24 East Basin Argo float salinity shallower than 10m vs salinity root mean squared (RMS) of piecewise linear, quadratic and mixed effect spline regression methods	38
Figure 25 8 th January 2012 OSTIA SST, Reconstructed SSS and associated error ranges	40
Figure 26 2 nd April 2012 OSTIA SST, Reconstructed SSS and associated error ranges	41
Figure 27 24 th June 2012 OSTIA SST, Reconstructed SSS and associated error ranges	42
Figure 28 Reconstructed OSTIA SSS correlation to Aquarius SSS over winter months (December, January, February and March) between December 2011 and March 2014	45
Figure 29 Time series of reconstructed OSTIA SSS and Aquarius SSS across three winters 2011-12, 2012-13 and 2013-14 from sites A, B and C	45
Figure 30 8 th January 2012 Aquarius 100km resolution SSS and reconstructed bin averaged 100km resolution SSS	46
Figure 31 2 nd April 2012 Aquarius 100km resolution SSS and reconstructed bin averaged 100km resolution SSS	46

1 Introduction

1.1 General Introduction to the Labrador Sea

The Labrador Sea is a location of open ocean deep convection (Marshall and Schott 1999). Through severe winter surface cooling ocean convection results in the formation of Labrador Sea Water (LSW), a cold-water mass that flows at intermediate depths along the western edge of the North Atlantic. LSW and deeper water masses flowing along the North Atlantic edge form the lower limb of the Atlantic Meridional Overturning Circulation (AMOC), a key component of the global climate system known as the “great ocean conveyor belt” (Broecker, 1991). The strength of the AMOC is of socio-economic importance as it redistributes heat, freshwater and carbon dioxide meridionally through the North Atlantic. In particular, the AMOC has been linked to Atlantic Multi-Decadal Oscillation and Sea Surface Temperature (SST) regulation, shown to have climatic impacts over Europe and beyond (McGeehan *et al*, 2011). When the AMOC is strong increased heat is transported to the North Atlantic, resulting in Europe and the Eastern seaboard of America becoming comparatively warmer than similar latitudes (Schmidt and Send, 2007).

1.2 Significance of Salinity

Salinity (S) is a challenging but critically important measurement in oceanography as changes in S when combined with temperature (T) determine the density of seawater. T and S are the basic properties of seawater and set during their most recent surface interval (Sundby *et al*, 2007). Despite mixing transforming water away from the surface, such properties can be reasonable conservative tracers of water masses and ocean currents (SPURS, 2012). In addition, ocean S is regarded as an important tracer of marine evaporation and precipitation, and recent satellite missions such as the Tropical Rainfall Measuring Mission highlight the importance of measuring ocean Sea Surface Salinity (SSS) to better measure these hydrological processes (Kummerow *et al*, 2010).

S and its vertical distribution is an indicator of convective conditions within the Western Labrador Sea (Lab Sea Group, 1998). Reduced convection weakens overturning and decreases northward transportation of saline waters. A number of recent studies have suggested that the high latitudes of the North Atlantic Ocean have been freshening over the last several decades (Robson *et al*, 2014; Glessmer *et al*, 2014). As a major location for deep water formation the Labrador Sea is sensitive to additions of freshwater, which act to stabilise (Solomon *et al*, 2007). Along with long term freshening, several wide spread fresh surface anomalies in the northern North Atlantic have been identified to occur. These “great salinity anomalies” (GSA) have been shown to occur nearly

once a decade and are thought to be due to long-lived icebergs south of 48°N, increased export of freshwater through Fram Strait (Dickson *et al*, 2002), extreme winters in the Labrador Sea (Belkin *et al*, 1998), enhanced freshwater outflow from the Canadian Arctic Archipelago or some combination of the above (Reverdin *et al*, 1997). These GSA's vary considerably both in their intensity and location. In the early 1970's S anomalies propagated anti-clockwise around the sub-polar gyre, whilst in another event in the 1980's they originated from within the Labrador Sea (Belkin *et al*, 1998). Findings associate such events with a significant reduction in Labrador Sea deep convection and North Atlantic Oscillation (NAO) index changes. For instance, the 1990 GSA occurred at the most negative NAO phase of the last 50 years (Sundby *et al*, 2007). Modelled experiments where large amounts of freshwater are added to the sub-polar North Atlantic, known as "hosing experiments", further support the theory of the AMOC being sensitive to freshwater, as they calculate a reduction in the formation of LSW (Kleinen *et al*, 2009).

1.3 New Era of Data

Collecting and analysing oceanographic data from satellites is a relatively new field of exploration. From satellites large areas of the oceans can be observed on useful timescales, and whilst expensive are considered worthwhile for the quantity of data collected across their lifetime. SST is accurately quantified from space by measuring long-wave radiation emitted by the molecular motion of the surface ocean (Reynolds *et al*, 2002). By combining multiple satellite SST and in situ based measurements a more complete coverage and accuracy to a fraction of a degree becomes achievable.

More recent developments in microwave remote sensing have allowed for SSS to be measured on a global scale. The standard practice of converting conductivity to salt concentration allows S to be remotely sensed from space. As the conductivity of ocean surface waters change (with S) there are minute detectable changes in the "brightness" of the ocean surface in microwave emissions. However, the scientific and technical complexity of this task is enormous due to the fact microwave emissions are sensitive to numerous other factors such as: SST, roughness, the intervening atmosphere and ionosphere and galactic signals reflected off the sea surface (Lagerloef *et al*, 2011). As a result, remotely sensed S is measured at an astronomically protected frequency band of 1.4 Ghz to reduce anthropogenic contamination (Boutin *et al*, 2013).

Prior to satellite data, most of what we understand about our oceans has come from infrequent and sporadic measurements collected by ships, buoys and drifters. These datasets often lack spatial and temporal coverage in

remote areas like polar and sub-polar oceans. However, more recently the broad-scale global array of T/S profiling floats, known as Argo floats, have grown to be a major component of the ocean observation system. Deployment of Argo floats began in 2000 and continues today at a rate of about 800 per year, providing a comprehensive and highly precise subsurface global ocean T and S dataset (Bowen *et al*, 2014).

1.4 Study Research Aims

Currently a data gap exists in S measurements as satellite derived S data is of coarse resolution and low precision, whilst contrasting in-situ Argo float data offers high precision measurements, but lack in spatial and temporal coverage. As the surface layers of the Labrador Sea tend to be both fresh and cold, the aim of this paper is to answer whether a correlation exists between Argo float T and S data to allow a high precision SSS look up table to be produced. If so, higher resolution SSS maps than the currently available 100km² gridded satellite datasets could be derived from infrared SST satellite measurements or multi-SST products, typically ~5km² in spatial resolution and on more useful timescales. The ability to reconstruct SSS from SST may not only produce a high resolution dataset but additionally provide an insight into freshwater exchanges that escape boundary currents and reach the interior Labrador Basin, seasonal salinity cycles and major regions of interest (e.g. locations of deep convection). The potential applications of such a SSS lookup table are broad within this socio-economically important region and could benefit numerous scientific studies.

2 Background

The interest in retrieving S from T observations is not a new concept in oceanography. Emery (1975 and 1976) reports on the work of Henry Stommel, who used T–S relationships to estimate dynamic height back in 1947. Stommel recognised that the co-variability of S with T could be exploited to estimate S with the basic idea that much of S variability is due to vertical displacements of water with relatively well-defined T and S properties. Thus the S that can be expected for a given T is essentially what was previously observed at the same T (Meijers *et al*, 2011).

Since S estimation from climatological T data was first put forward a number of variations from this basic method have been proposed to extend its scope of application (Hansen *et al*, 1999). A study by Ballabriga-Poy (2009) focused on the reconstruction of S in the upper 1200 m of the eastern North Atlantic Ocean, a region characterised by the presence of many different water masses, in some cases similar to the Labrador Sea. Whilst a previous study by Marrero-Díaz *et al*, (2006) found it necessary to split this region into boxes and fit individual

climatological models, Ballabrera-Poy (2009) implemented an adaptable Gravest Empirical Mode (GEM) regression to analyse the sub-surface region as a whole. This approach used knowledge of geographical location (latitude and longitude), T and SSS (where present), all thought to contain S information to better estimate ocean S. The predictor of geographical location (latitude and longitude) notably acted to reduce errors most substantially when vertically reconstructing S. The study went on to identify the upper 50m of the water column to be the most erroneous and difficult to estimate, due to large seasonal fluctuations in S and external forcing by freshwater. Where SSS observations were absent measurements were reconstructed from surface Conductivity Temperature and Depth (CTD) T and S measurements. However, this T-S reconstruction was only carried out in several small locations and based on a handful of CTD measurements and analysed using a single quadratic regression. Nonetheless these case studies highlight the challenges of SSS reconstruction across a large spatial area prone to large variability in T-S relations from water depth, long-term trends and external forces.

Another study by Thacker *et al*, (2007) focused on the reconstruction of vertical S from T in the Gulf of Mexico. The authors chose this region for several reasons; firstly, its geographical separation from the Caribbean Sea and North Atlantic Ocean makes it a ‘small ocean’, characterised by a deep central basin surrounded by substantial continental shelf. Secondly, a relatively large number of CTD profiles have been performed in the region over a 6-year period (2000-2006), providing enough spatial and temporal data coverage to construct an empirical T-S relation. Finally the relationship between T and S was found to be sufficiently regular that a single empirical model could be used to estimate S. The single model applied four linear regression lines to represent the T-S relationship at all depths including the surface. Thacker *et al*, (2007) went on to conclude that an ideal region to next explore would be a large, highly variable area of importance to ocean circulation, potentially in the North Atlantic. The Labrador Sea fits into this category perfectly, with a deep central basin, reasonably covered by Argo float profiles and important to North Atlantic circulation.

3 Data

3.1 Argo Floats

The Argo array is an international collaboration that collects high-quality T and S profiles from the upper 2000m of the ice-free global ocean. The data comes from battery-powered autonomous floats drifting at depths of ~1000m where they maintain neutral buoyancy to surrounding ambient seawater. Numerous Argo float models

are present, but typically on 10-day intervals the floats pump fluid into an external bladder and rise to the surface over ~6 hours while measuring T and S (Argo, 2014; Roemmich *et al*, 2009). Satellites determine the position of the floats when they surface, and the floats transmit their data to the satellites. The bladder then deflates causing the float to sink to its ‘parking-depth’ until the cycle is repeated. Floats are designed to make about 150 cycles across their life span (Boutin *et al*, 2013). The main strength of using a dataset such as Argo floats is measurement uncertainties are expected to be less than 0.005°C for T and 0.01 for S, making them an ideal dataset for documenting minute changes in large-scale S fields within this study (Roemmich *et al*, 2009).

Delayed Argo float T and S data, subject to additional scrutiny by oceanographic experts and S adjusted against high quality ship-based CTD data has been used in this study. Measurements between (50°N, 65°W - 70°N, 45°W) and January 2002 - December 2012 were downloaded from <http://odc.noaa.gov/argo/> accessData.htm and across this time period the size of the Argo array was noted to progressively increase. Additional quality control was performed to remove further errors, spikes or bad profiles. Several studies have used a personal quality control before (e.g. [Levitus, 2000; Roemmich, 2009; Willis *et al*, 2004; Ivchenko *et al*, 2010]). However, these studies eliminate entire profiles from the data set if a point of that profile is 2–6 standard deviations from the monthly climatology. Instead single points from a profile have been eliminated if they existed outside of the range (T >23 and <-2.5, and S >35.7 and <27) or showed obvious T/ S spikes.

3.2 Combined Satellite and In-situ SST

The Operational Sea Surface Temperature and Sea Ice Analysis (OSTIA) is a level 4 Global Grouped High Resolution SST (GHRSST) dataset produced daily on an operational basis at the UK Met Office using optimal interpolation on a global 0.054 degree (~5km) grid (Stark *et al*, 2007). The compiled dataset uses SST satellite data from sensors that include the Advanced Very High Resolution Radiometer (AVHRR), the Advanced Along Track Scanning Radiometer (ATSR), the Spinning Enhanced Visible and Infrared Imager (SEVIRI), the Advanced Microwave Scanning Radiometer-EOS (AMSRE), the Tropical Rainfall Measuring Mission Microwave Imager (TMI), and in situ data from drifting and moored buoys (Donlon, 2006).

Daily OSTIA data between (50°N, 65°W - 70°N, 45°W) August 2011-February 2015 have been used and is readily available from the UK Met Office Website: http://ghrsst-pp.metoffice.com/pages/latest_analysis/ostia.html. The use of level 4 data, based on multiple sensors and sensor types, reduces associated SST errors from individual sensors or instruments.

3.3 Satellite SSS

Aquarius is a near polar sun synchronous orbit satellite mounted upon the SAC-D platform. The SSS Aquarius instrument is the first mission with the primary goal of measuring SSS from space. The instrument carries 3 radiometers and 1 scatterometer, operating in the microwave L band at 1.4 GHz & 1.2 GHz respectively (Boutin *et al*, 2013). The data collected by the radiometer is used together with SST collected by numerous other platforms and corrected for surface roughness measured by an on-board scatterometer, to derive S. The level 3 SSS data used in this study is gridded at 100km resolution and a daily temporal resolution. Aquarius only achieves global SSS coverage every 7 days, so to achieve a global SSS dataset at daily resolution 7 days of data must be considered and pushed back to the first day, creating an overlap in data measurements. Across a 7 day period and after level 3 data processing Aquarius SSS measurements have an accuracy of ~0.9.

Daily Aquarius data between (50°N, 65°W - 70°N, 45°W) August 2011-February 2015 has been used in this study as a means of comparing reconstructed SSS values to an existing SSS dataset, and is readily available from the National Aeronautics and Space Administration (NASA) Website: <http://podaac-opendap.jpl.nasa.gov/opendap/allData/aquarius/>.

4 Variability of Surface Temperature and Salinity from Argo

4.1 Argo Float Surface Representation

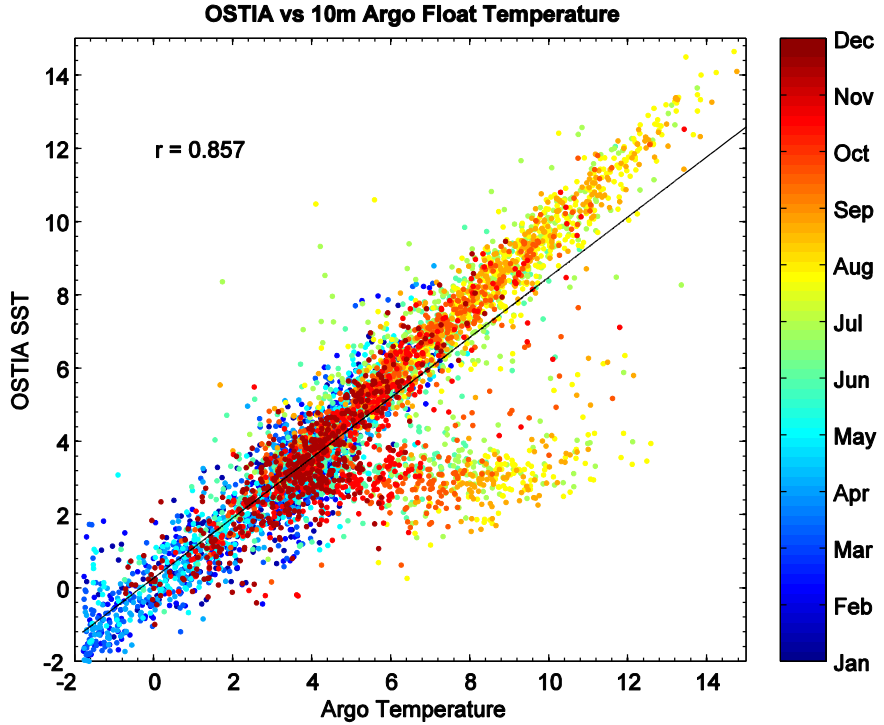


Figure 1 | January 2002 - December 2012 Argo float temperature measurements shallower than 10m vs nearest OSTIA level 4 SST. Marker colour represents month of the year, whilst the r value and linear regression indicate data correlation.

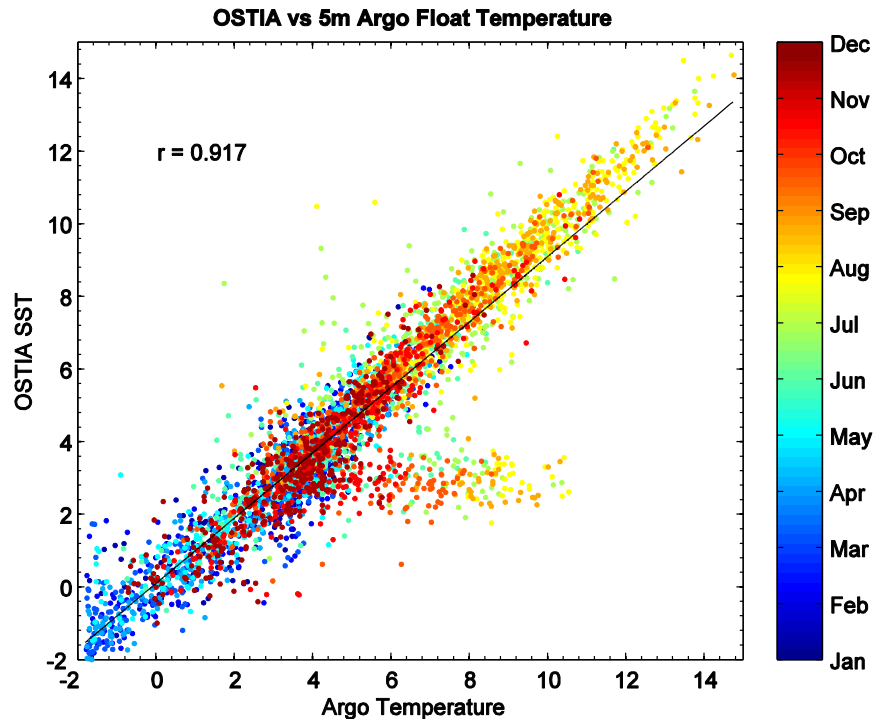


Figure 2 | January 2002 - December 2012 Argo float temperature measurements shallower than 5m vs nearest OSTIA level 4 SST. As figure 1, for shallower than 5m Argo measurements.

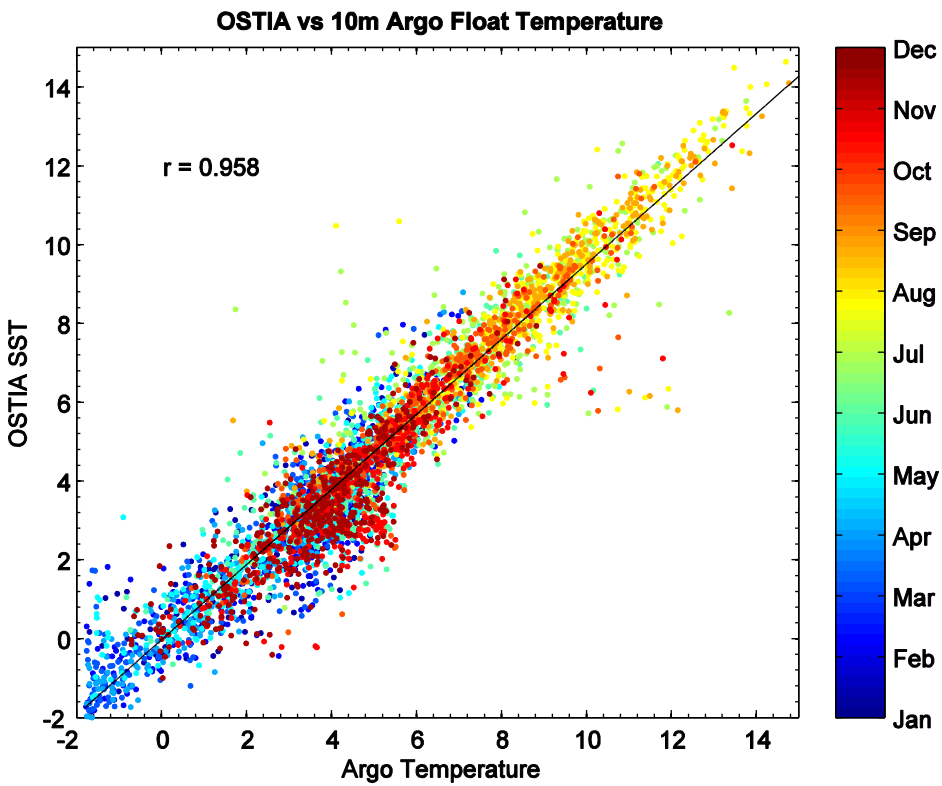


Figure 3 | January 2002 - December 2012 Argo float temperature measurements shallower than 10m with Argo profiles removed vs nearest OSTIA level 4 SST. Marker colour represents month of the year, whilst the r value and linear regression indicate data correlation.

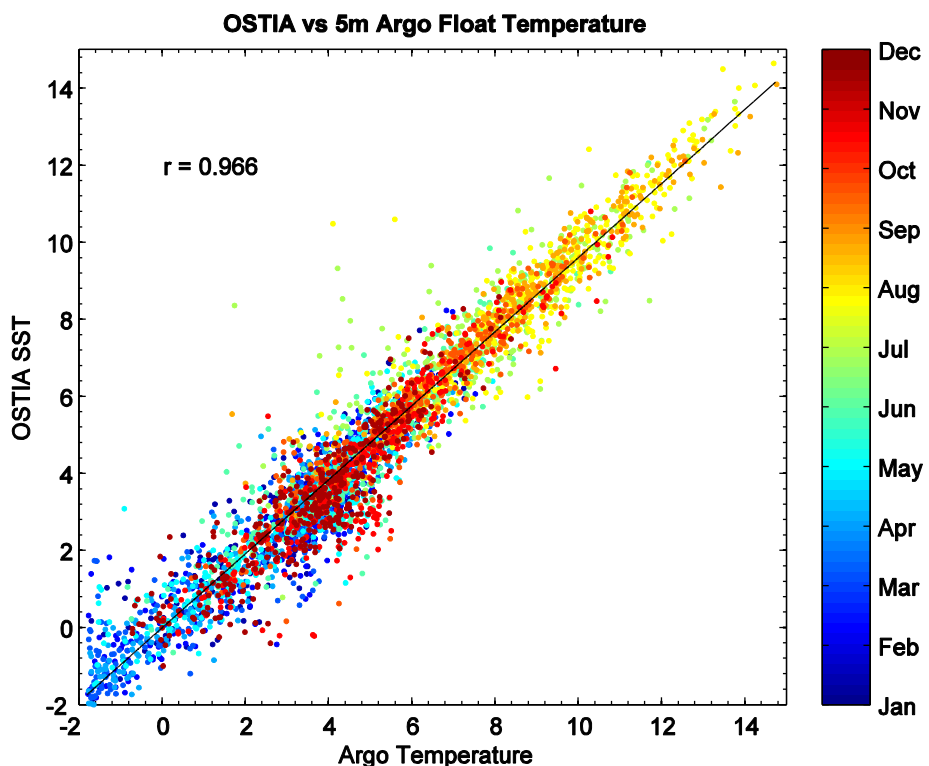


Figure 4 | January 2002 - December 2012 Argo float temperature measurements shallower than 5m with Argo profiles removed vs nearest OSTIA level 4 SST. As figure 3, for shallower than 5m measurements (with profiles removed).

How well near surface Argo float T measurements compared to true surface T values (Level 4 OSTIA data) must be considered before constructing a climatological T-S relation from Argo float data to represent surface waters of the Labrador Sea. In the study region (50°N, 65°W - 70°N, 45°W) the 6734 Argo float measurements had their shallowest surface measurements in the top 48m. Of these, only 5742 profiles had a surface measurement shallower than 10m, indicating 992 of ‘surface’ measurements have been collected deeper than 10m. Further still, only 4393 profiles had a surface measurement shallower than 5m. Figure 1 and 2 illustrate both shallower than 10m and 5m T shows a strong correlation to OSTIA SST measurements (r values of 0.86 and 0.92, respectively). Measurements collected down to depths of 5m as anticipated demonstrate a better correlation to surface T than measurements collected down to depths of 10m. Both datasets follow a similar linear relationship; however shallower than 10m T measurements demonstrate a larger data scatter about the linear trend.

A point of interest on figures 1 and 2 is the unusual occurrence of warm Argo T values, predominantly between July-October, when OSTIA SST at the same location and time remain uniformly cold (at ~4°C). Further analysis identified these Argo floats were random in both location and time but shared five common Argo float numbers (Call ID: 49068, 4901406, 4900528, 4900531 and 4901445). T measurements collected by these Argo floats deviate substantially from the strong linear relationship followed by the remainder of data points, possibly due to calibration issues or another underlying unknown reason, and so have not been included in further analysis. Upon removal of these Argo measurements the mean sampling depth remains relatively consistent for both T datasets (at 4m and 4.8m for $\leq 5\text{m}$ and $\leq 10\text{m}$ T, respectively) and the correlation improves to r values of 0.96 for both datasets.

Separating data points by time of year suggests cold Autumn-Winter T values converge about the linear fit, whilst warm summer T data points undercut the line (figures 3 and 4). Intermediate T values during June and July illustrate the largest variability about the fitted regression, noticeably extending to both warmer OSTIA T values and colder Argo T values. The tendency for winter Argo T and OSTIA SST at both $\leq 5\text{m}$ and $\leq 10\text{m}$ to agree implies a well-mixed water column exists, whilst summer disagreement between Argo T and OSTIA SST, most notably towards warmer OSTIA SST, suggests stratification may be present.

Minimal difference between ≤ 5 m and ≤ 10 m summer T ‘spread’ about the fitted regression suggests stratification is shallower than 5m but also implies either dataset is a suitable surface representation. Argo T measurements ≤ 10 m demonstrate as strong a correlation to OSTIA SST as ≤ 5 m measurements and have an average sampling depth only 0.8m deeper. Additionally the 5742 ≤ 10 m measurements, after Argo float removal, provides a larger sample size preferable for T-S relation analysis. For these reasons shallower than 10m measurements have been used in further analysis.

4.2 Temporal Variability and Long Term Trends

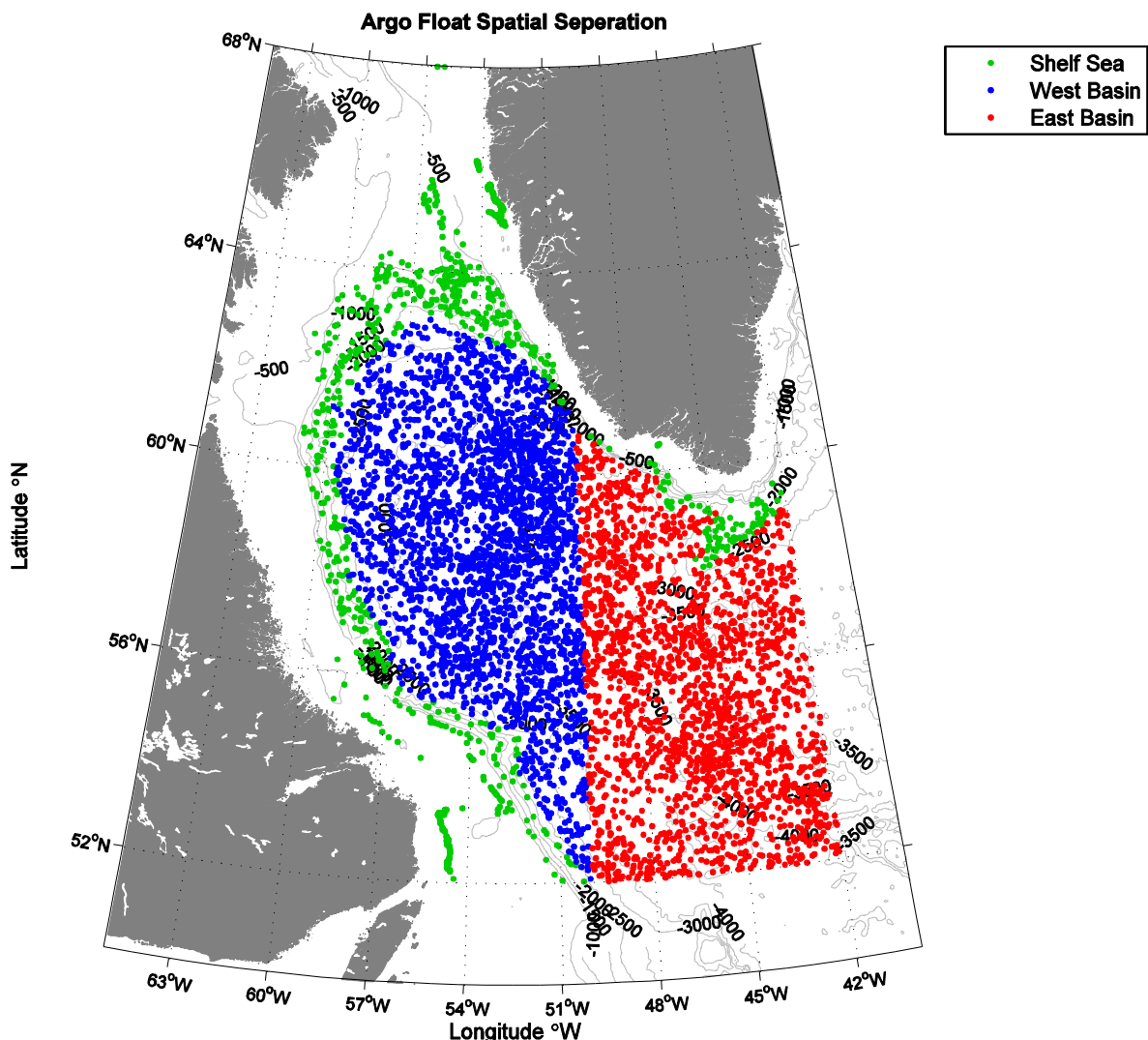


Figure 5 | January 2002 - December 2012 Argo profile locations shallower than 10m (post Argo profile removal). Green markers show profiles collected in waters shallower than 2000m, deemed to be on the near continental shelf. Blue markers are performed in waters deeper than 2000m and West of 45°W , and red markers are deeper than 2000m and East of 45°W .

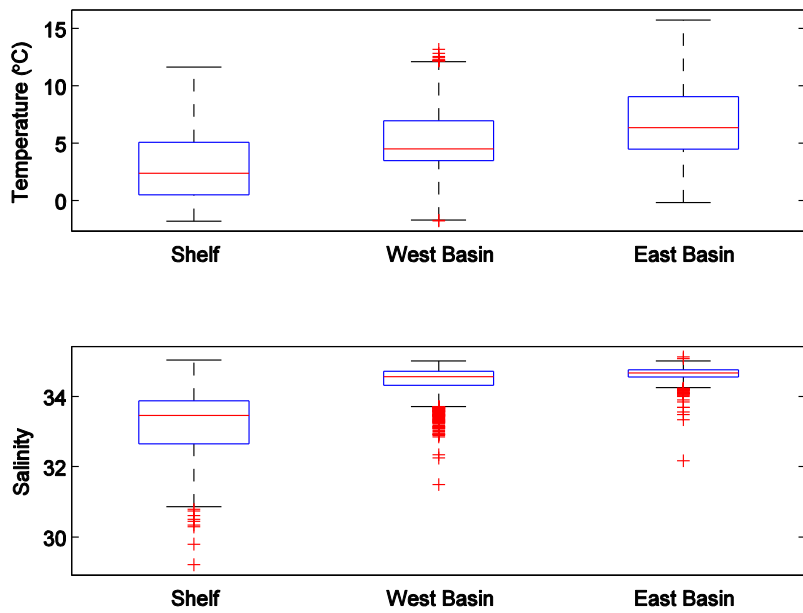


Figure 6 | Box and whisker diagrams of temperature and salinity of classified Shelf, West Basin and East Basin regions. Based on regions in figure 5.

A total of 5742 measurements shallower than 10m between January 2002 and December 2012 have been used in further analysis (Figure 5). Argo float measurements in waters deeper than 2000m and east of 45°W have been categorised as the East Basin (consisting of 987 data points). The longitude of 45°W, the most southerly point of Greenland, is used to separate the Labrador Sea and the North Atlantic. Measurements in waters deeper than 2000m and west of this longitude have been categorised as the West basin (consisting of 4867 data points). The remaining 880 data points of Argo measurements situated in waters shallower than 2000m, are considered to be on the near continental shelf. Such measurements are deemed to provide an inadequate representation of the continental shelf due to the comparatively small sample size and bias towards ~89% of measurements being collected in waters between 1700-2000m in depth. Although the separation of Argo measurements into East and West regions permits limited spatial variability it does improve the relationship between T and S by reducing the spread of values. All regions demonstrate a similarly large range in T, whilst S variability appears more region specific (figure 6). Based on the limited data available, shelf seas demonstrate the largest fluctuation in S (ranging from ~34.8 – 29.3 when fresh outliers are considered in figure 6). In comparison S varies far less within the West and East basin, and S variability is particularly minimal within the East Basin due to strong influence of the North Atlantic east of 45°W.

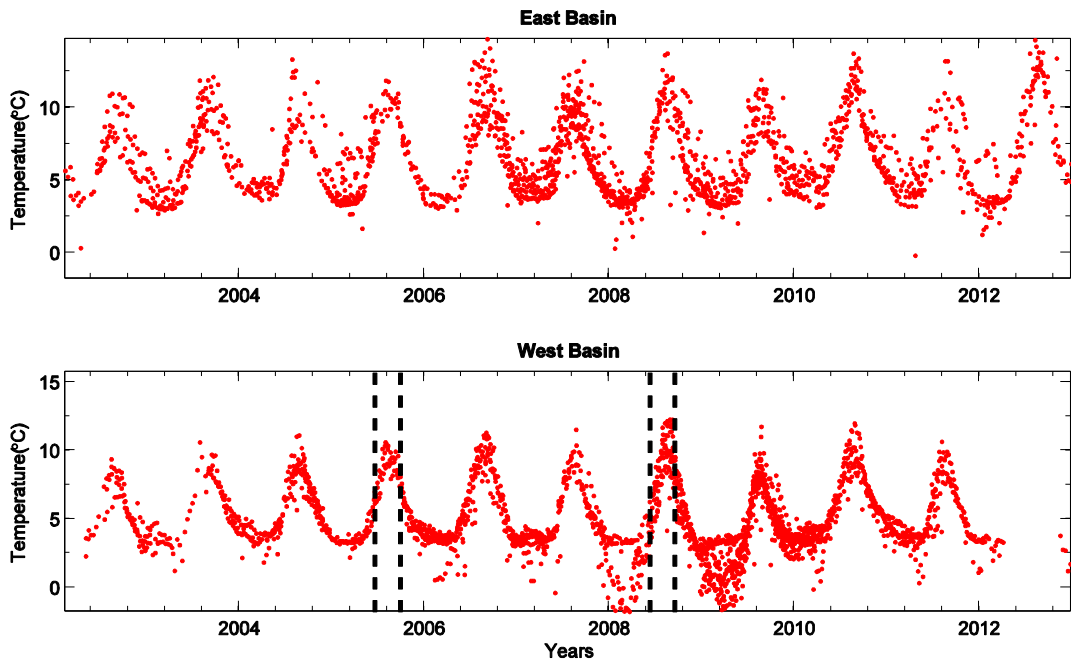


Figure 7 | January 2002 - December 2012 time series of East and West Basin Argo float temperature collected shallower than 10m, illustrated in figure 5. Dashed black lines illustrate 2005 and 2008 summer months analysed in figures 9 and 10.

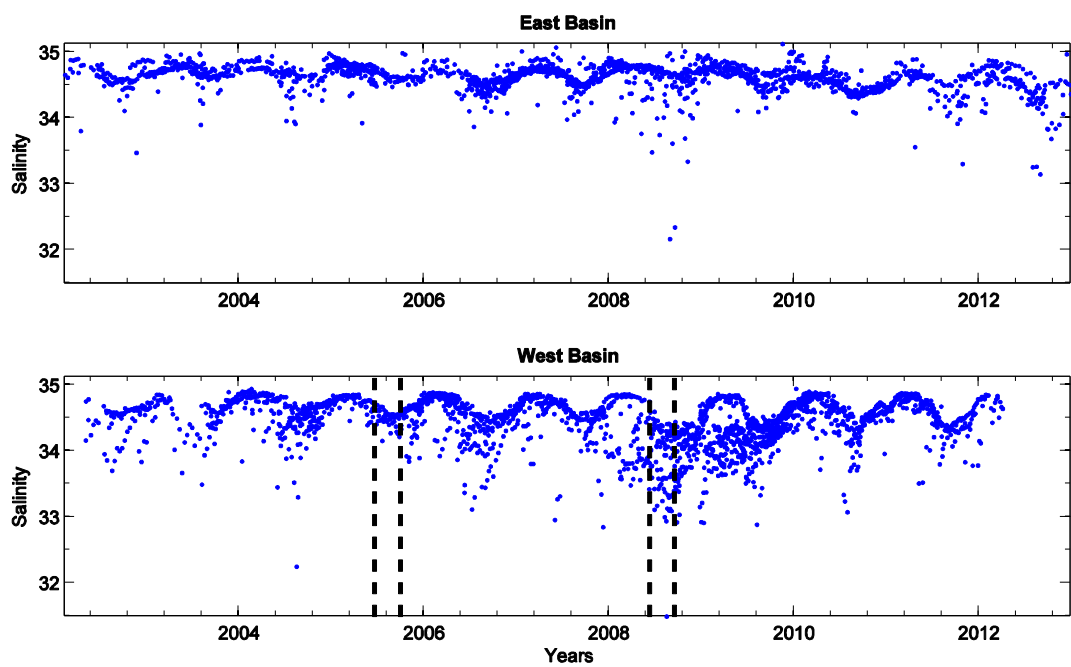


Figure 8 | January 2002 - December 2012 time series of East and West Basin Argo float salinity collected shallower than 10m, illustrated in figure 5. Dashed black lines illustrate 2005 and 2008 summer months analysed in figures 9 and 10.

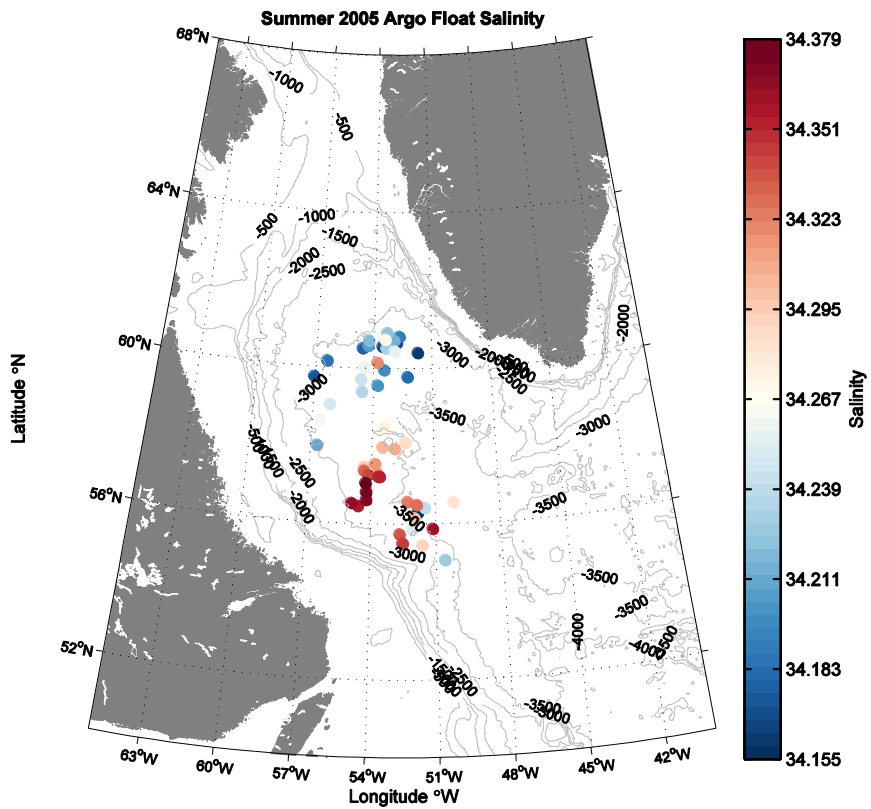


Figure 9 | West Basin Argo float profile locations and corresponding salinity during summer months (December, January, February and March) of 2005, illustrated as black lines in figure 8.

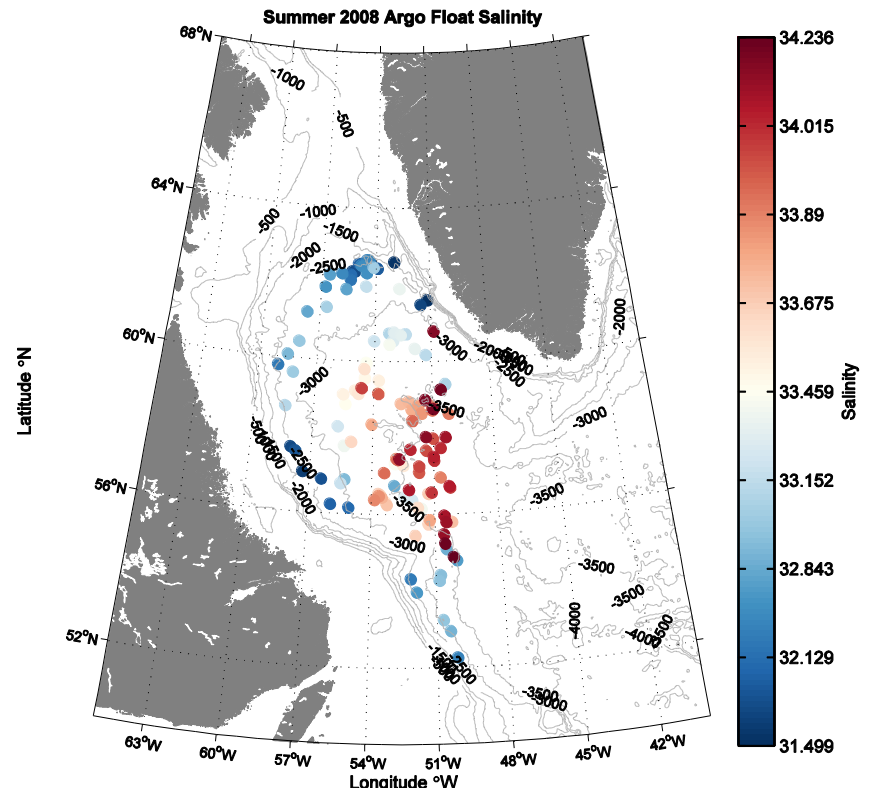


Figure 10 | West Basin Argo float profile locations and corresponding salinity during summer months (December, January, February and March) of 2008, illustrated as black lines in figure 8.

Analysis of ‘surface’ T and S within the East and West Labrador Basin is illustrated in figures 7 and 8. T and S can be seen to oscillate in anti-correlation to one another seasonally across both divisions of the basin. In summer months, waters are relatively warm and fresh compared to winter months. These regional time series indicate S has a smaller seasonal range than T across both regions. However, numerous low S measurements visibly occur over summer months in both regions, but most notably the West Basin.

A point of interest is that multiple oscillations in T are present in the West Basin over the winters of 2008-09 and 2009-10. Two substantial surface cooling events appear to have occurred in these years, evident by Argo float ‘surface’ T measurements dropping to $\sim 1.2^{\circ}\text{C}$. However, S values appear to remain reasonably constant, implying these cooling events are little problem for estimating S from T.

The locations of Argo floats during a uniformly high S summer (2005) and low S summer (2008) within the West Basin are shown to differ considerably (figures 9 and 10). In 2005 Argo floats are situated closer to the central Western basin, whilst in 2008 they are evidently closer to the fresher boundary currents. A strong horizontal S gradient in 2008 of ~ 1.5 is visible between Argo floats within/close to boundary currents and the central Western Basin, a $\sim 800\text{km}$ distance. This implies the growth in the Argo float community and variability in Argo location appear to be the main reason for observed fresh S values and not long term freshening, which cannot necessarily be implied from Argo data. Based on these findings the East Basin illustrates a less sporadic annual T and S fluctuation than the Western Basin, which is most likely due to a more stable influence from the North Atlantic and less Argo floats being close to boundary currents.

5 Monthly Temperature-Salinity Relationship

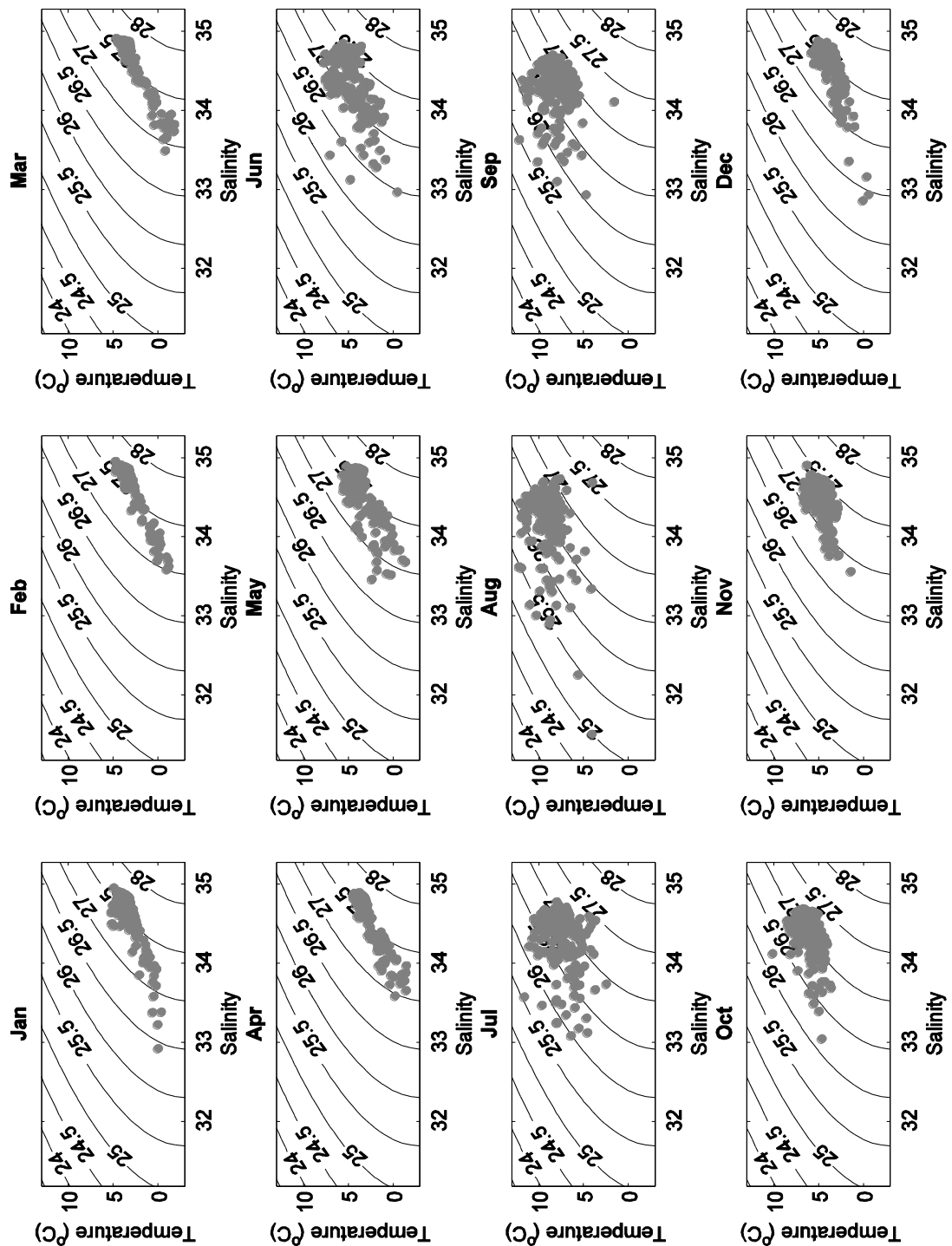


Figure 11 | West Basin Argo float shallower than 10m temperature and salinity monthly diagrams overlaid onto seawater density contours.

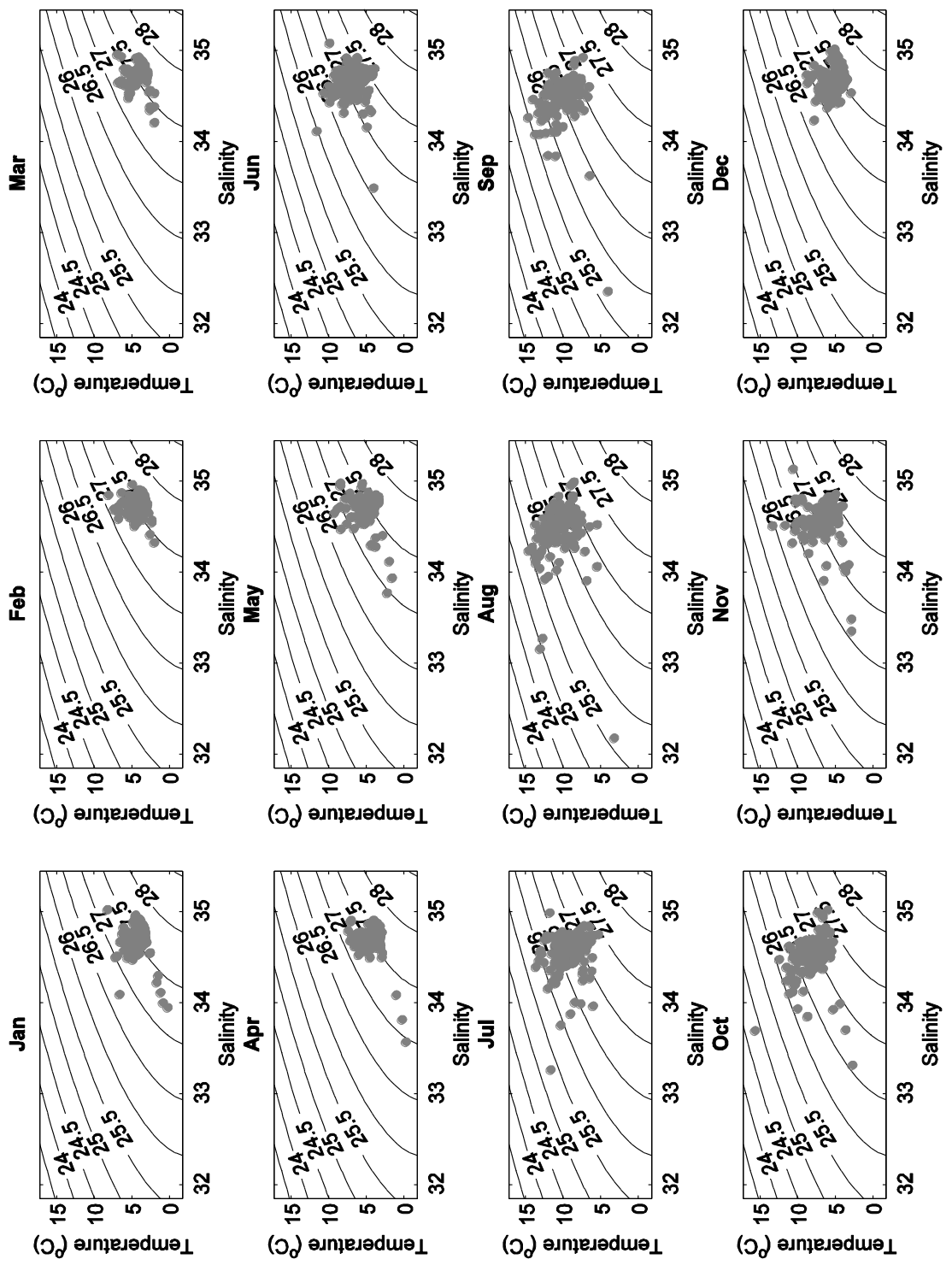


Figure 12 | East Basin Argo float shallower than 10m temperature and salinity monthly diagrams overlaid onto seawater density contours.

Table 1 / Monthly mean, and annual mean and standard deviation (SD) based on monthly means in temperature and salinity for the East and West Basin, based on figures 11 and 12.

Month		Jan	Feb	Mar	Apr	May	Jun	July	Aug	Sep	Oct	Nov	Dec	Annual Mean	SD
East Basin	Temp °C	4.36	4.27	4.09	4.30	5.06	7.06	9.25	10.37	9.95	8.02	6.64	5.21	6.54	2.35
	Sal	34.70	34.73	34.73	34.71	34.69	34.64	34.56	34.46	34.46	34.51	34.54	34.68	34.62	0.10
West Basin	Temp °C	3.23	3.04	2.74	2.81	3.32	4.73	7.51	8.96	8.15	6.11	4.70	3.57	4.91	2.23
	Sal	34.60	34.63	34.61	34.58	34.51	34.36	34.30	34.18	34.27	34.35	34.47	34.51	34.45	0.15

T-S diagrams (figure 11 and 12) show substantial seasonal and spatial variability exists over the 10 years of Argo measurements. Within the West Basin (figure 11), winter and spring months (December - April) demonstrate a nearly linear relationship, with low S values corresponding with low T values and a small range in S at specific T intervals. By May this T-S relationship alters; data points begin to spread away from the narrow near linear relationship, creating a consequently larger range in S values at T intervals. From May – August the relationship between T and S begins to progressively ‘breakdown’, evident by the large range in S values across most T values, implying S is not in accordance with T. The ‘breakdown’ occurs roughly around the time of the vernal equinox, peaking in August and persisting until around the winter solstice. From August to November, T and S begin to return to a well-defined positive near-linear relationship about colder and more saline values.

Although fewer measurements are present in the East basin a strong T-S relationship is still illustrated (figure 12). The relationship visibly differs from the T-S relation seen in the West Basin, with winter months following less of a linear relationship and months in the second half of the year even demonstrating an inverted relationship; where low S values occur at high T values and vice versa (particularly in August, September, October and December). Additionally, the average S value across all months is noticeably higher than the West Basin (with an annual mean S of 34.62) and is seen to vary less between months due to a strong saline North Atlantic influence (evident by the lower standard deviation of 0.1, table 1). Whilst the T-S relation itself visibly differs the annual trend is consistent with the West Basin, where winter and spring months demonstrate a well-defined relationship before ‘breaking down’ between March and December. Causing a relatively sporadic relationship to exist over these months, where high and low S values are not confined to a specific T values, posing a problem for estimating one from the other.

Within the West Basin lowest summer S values appear to occur at cold T values. However, between May and August only ~8% of these S measurements are fresher than 32.5, indicating few low summer S measurements exist across the 10 year period. In contrast, the lowest summer S values in the East Basin occur at warmer T values; although as highlighted previously, the sporadic distribution of Argo floats across the 10-year period most likely means such measurements have been collected close to the fresh continental shelf boundary currents.

6 Quantifying the surface T-S relationship

6.1 Upper and Lower Bounds

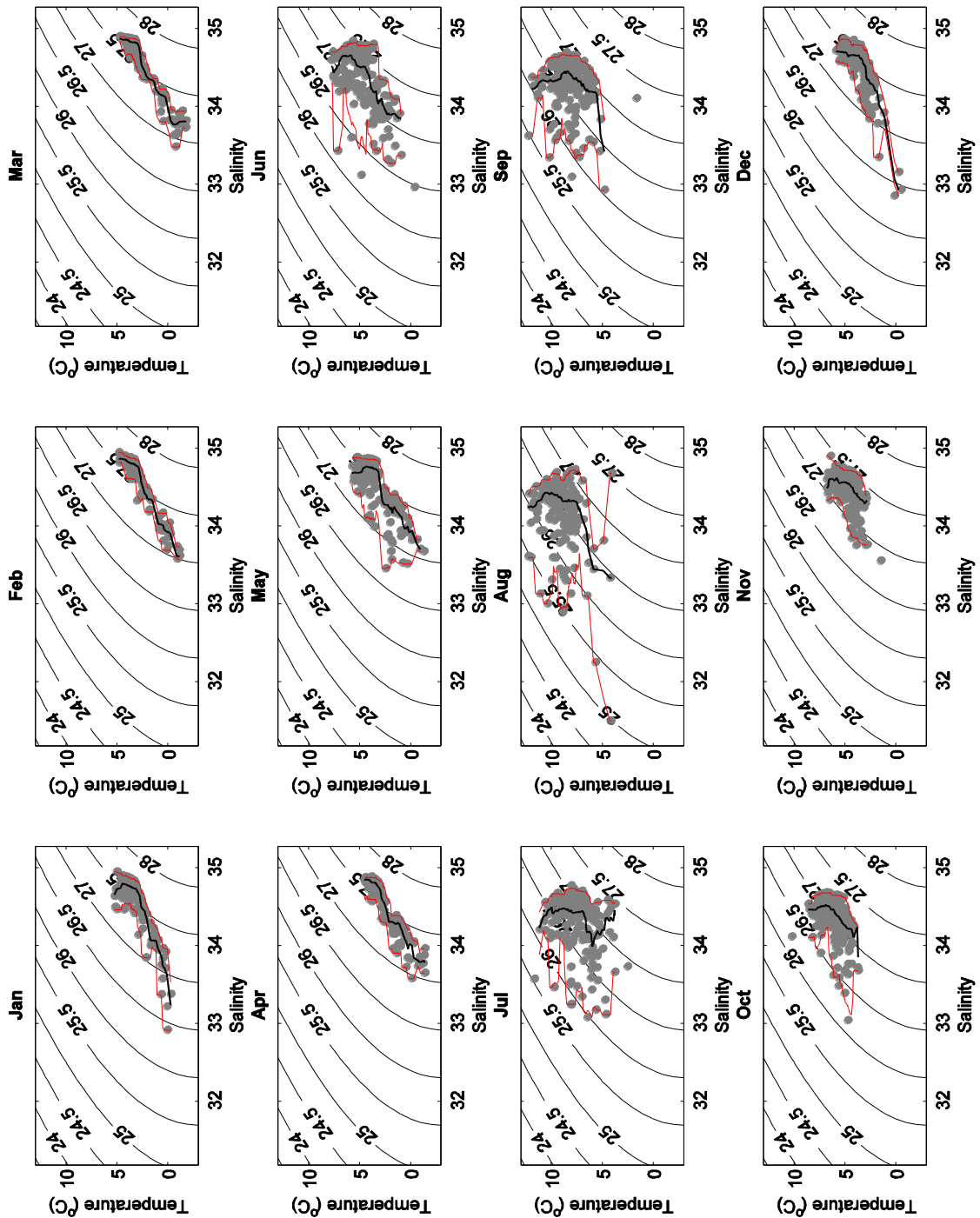


Figure 13 | West Basin Argo float shallower than 10m temperature and salinity monthly diagrams overlaid onto seawater density contours. The two red lines illustrate the 5% and 95% salinity percentiles and the black line the median, all within overlapping 0.5°C bins incremented by 0.1°C .

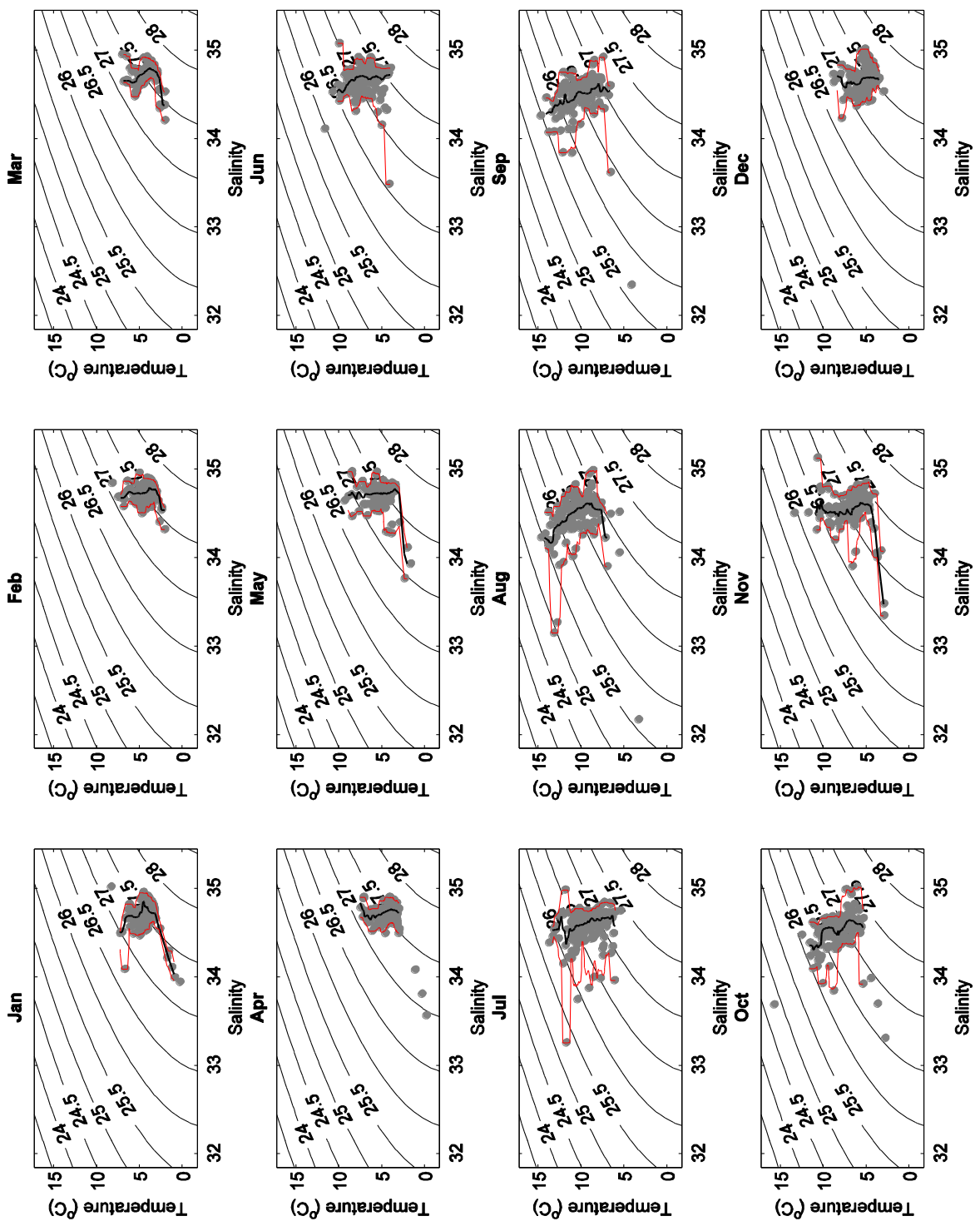


Figure 14 | East Basin Argo float shallower than 10m temperature and salinity monthly diagrams overlaid onto seawater density contours. As figure 13, for the East Basin.

For each set T, the spread of S values shown to occur across 10 years of Argo data can be used to identify associated errors. The previous chapter identifies a nearly linear relationship within the West basin, whilst a less well confined relationship exists in the East Basin, which becomes inverted around June. For a normally distributed dataset about the mean, the 95% confidence intervals could be calculated from the mean \pm 2 standard deviations. However, the positively skewed distribution of all monthly S datasets towards higher S values, results in such a method overestimating the upper 95% limits due to the mean being skewed towards higher S values and not centrally within the data distribution (Emery and Thompson, 2001). For the non-normally distributed datasets I use 5% and 95% percentiles as lower and upper error bounds respectively, to represent where the majority 90% range in monthly S with T lies. The percentiles were calculated from Argo float S values within overlapping T intervals of 0.5°C that are incremented at 0.1°C . Allowing bins to overlap retains enough S measurements to gain a reliable representation of S ‘spread’ at 0.5°C T intervals. The upper and lower bounds are not calculated for T intervals where fewer than two S measurements are present to prevent inaccurate data representation. Finer intervals than 0.5°C would result in more variable bounds, whilst the use of a coarser bin size would smooth out the upper (95%) and lower (5%) bounds and span T intervals where few S measurements exist.

The range in S between the upper and lower bounds at a given T value represents where 90% of S data collected across 10 years exists. The upper and lower bounds are closely confined to the median in winter, spring and autumn months in both the East and West Basin (figures 13 and 14). However, the bounds are evidently closer to one another in the West Basin when the T-S relation is nearly linear, compared to the non-linear East Basin relations. A large deviation in the lower bound towards lower S values noticeably occurs in summer months of both regions due to the presence of numerous low S values, resulting in large associated errors.

6.2 Methods for T-S Transfer Relationship

Here 3 methods have been used; a piecewise linear, quadratic and mixed effect spline regression to try and represent monthly T-S relations. The variable nature of the T-S relationship between months and regions makes it difficult to apply a single universal method, and choosing the appropriate order and number of regression lines is important to ensure data are well represented.

6.2.1 Linear Regression

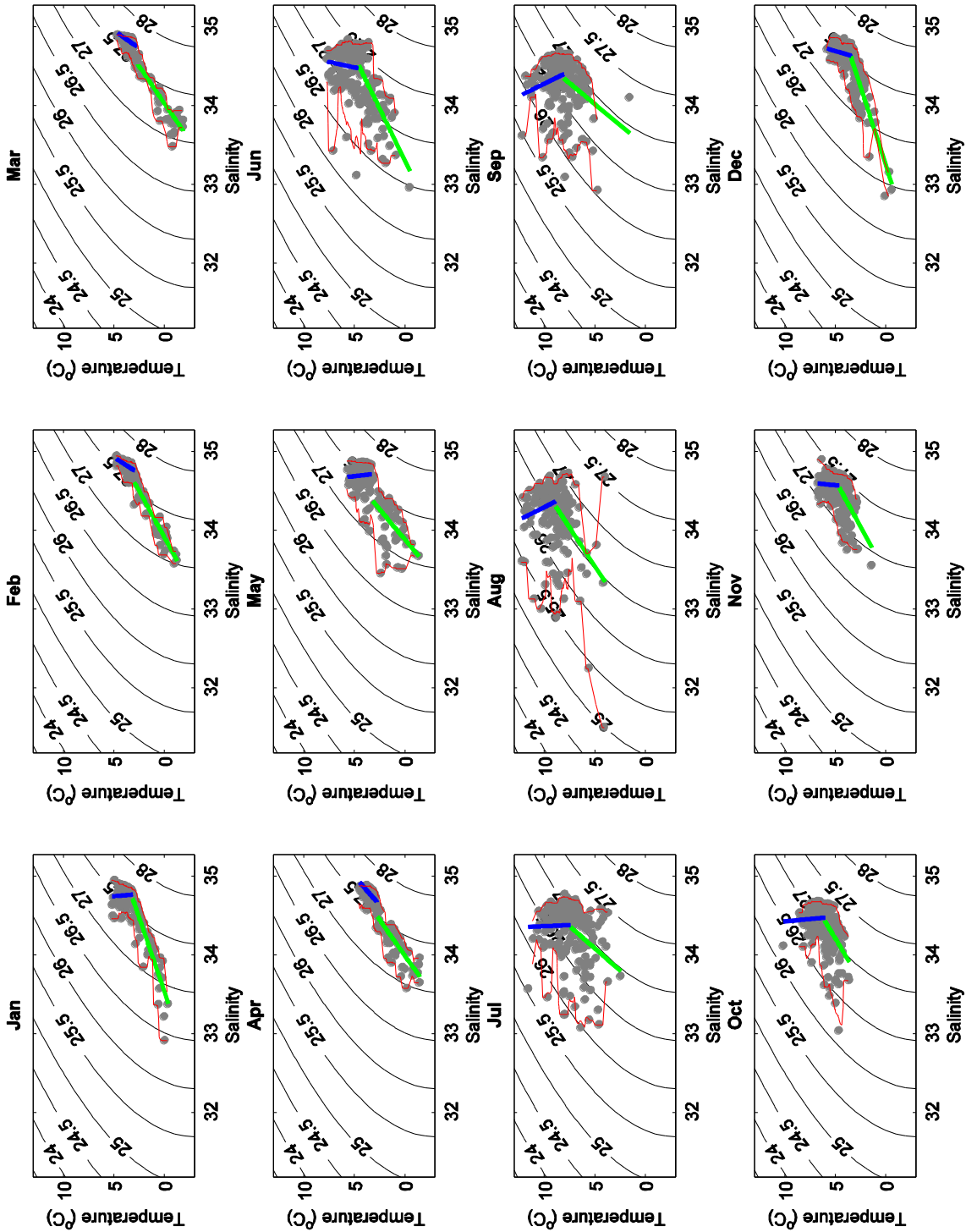


Figure 15 | West Basin Argo float shallower than 10m temperature and salinity monthly diagrams overlaid onto seawater density contours. The two red lines illustrate the 5% and 95% percentiles, and the blue and green lines illustrate two separate linear best fit regression lines for each month. The blue line is fitted to temperature and corresponding salinity values greater than the mean monthly temperature, whilst the green line is fitted to temperature and corresponding salinity values less than the monthly mean temperature.

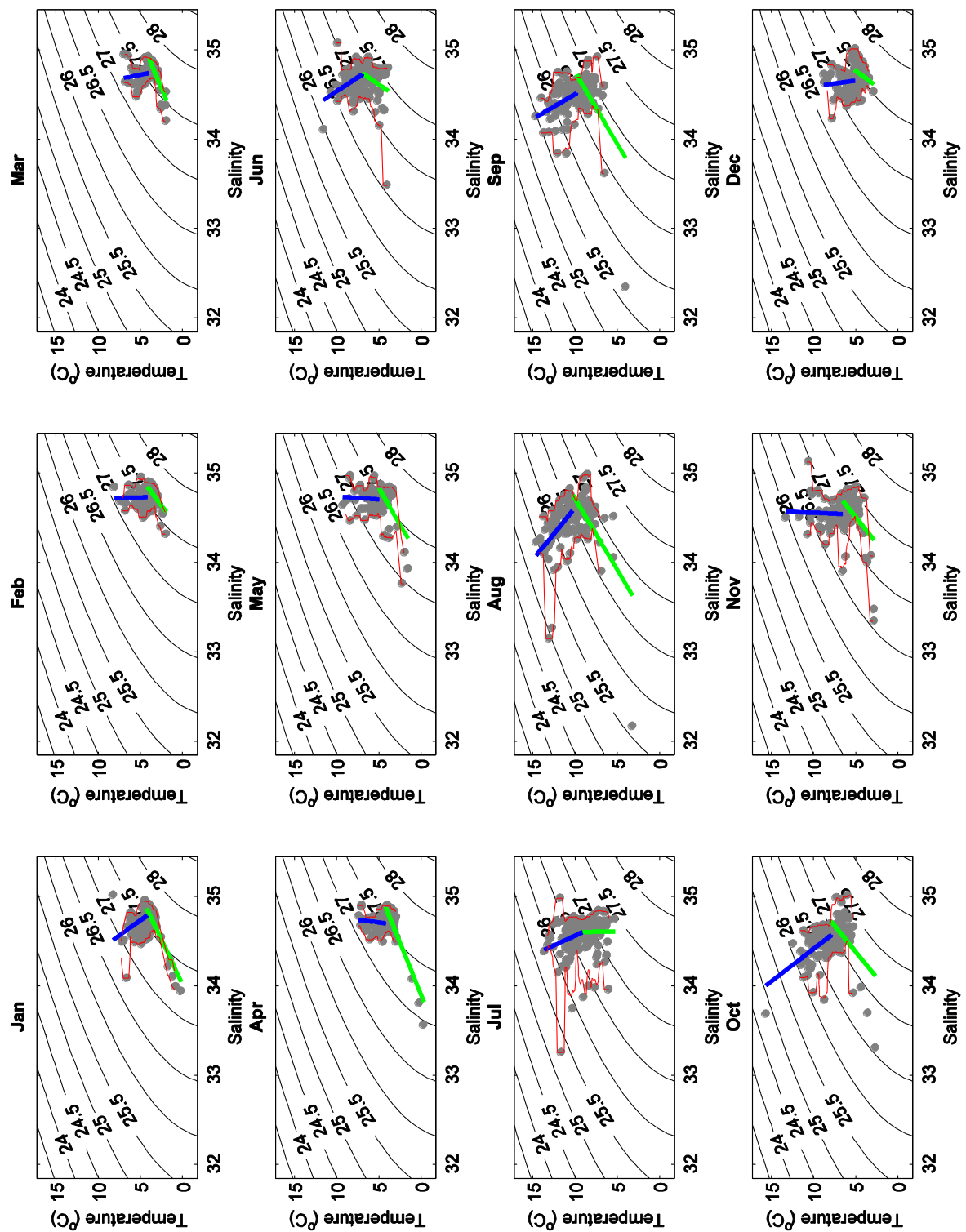


Figure 16 | East Basin Argo float shallower than 10m temperature and salinity monthly diagrams overlaid onto seawater density contours. As figure 15, for the East Basin.

Initially a piecewise linear regression, divided at the monthly mean T, was used to represent T-S data (figures 15 and 16). One linear regression was applied to S data above the mean T for each month and another was fitted to S data with corresponding T values colder than the monthly mean. Within the West Basin, particularly during winter months, the piecewise linear regression remains within the upper and lower bounds and agree well with underlying data. However, in the West Basin over summer months and the majority of months in the East Basin this method represents T and S data poorly. The T-S diagrams for these months additionally highlight the two regressions misalign at the mean monthly T, creating a large variability in S over a minor T difference. The piecewise linear regressions in a number of cases appears not to be confined to values within the upper and lower bounds, particularly where extreme S changes in the bounds occur or where bounds become narrow. This poses the problem of such a method, at certain times of year, predicting S values that do not agree with where 90% of Argo float measurements are present.

The use of the mean monthly T as the division point between lines also does not seem the best approach for all months, particularly those in summer experiencing a T-S ‘breakdown’. The single separation between linear regressions crudely illustrates T-S trends for all months within the East Basin and summer months within the West Basin, indicating the use of a more complex regression type would be better suited.

6.2.2 Quadratic Regression

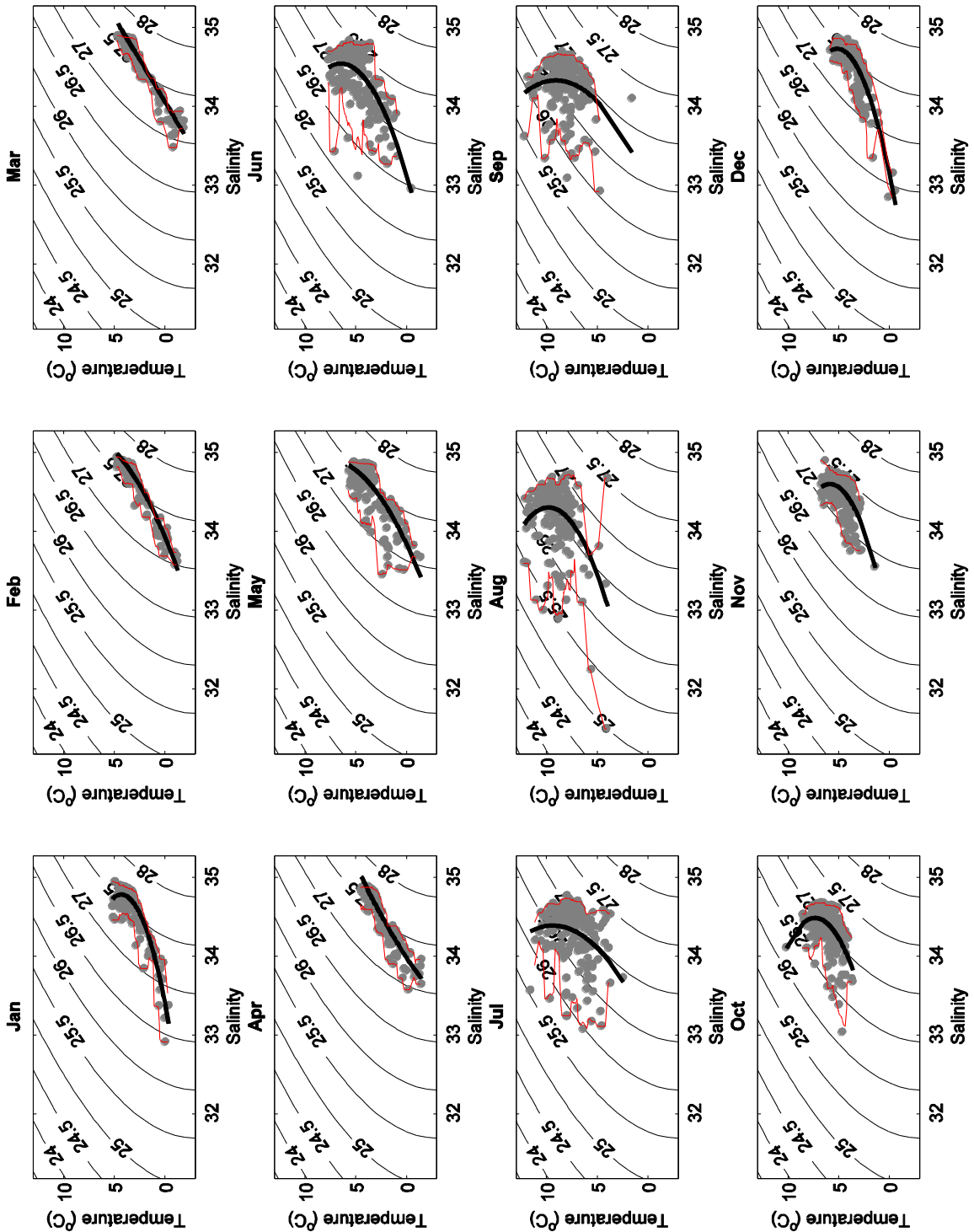


Figure 17 | West Basin Argo float shallower than 10m temperature and salinity monthly diagrams overlaid onto density contours. The two red lines illustrate the 5% and 95% percentiles and the black lines illustrates a single best fit quadratic regression for each month.

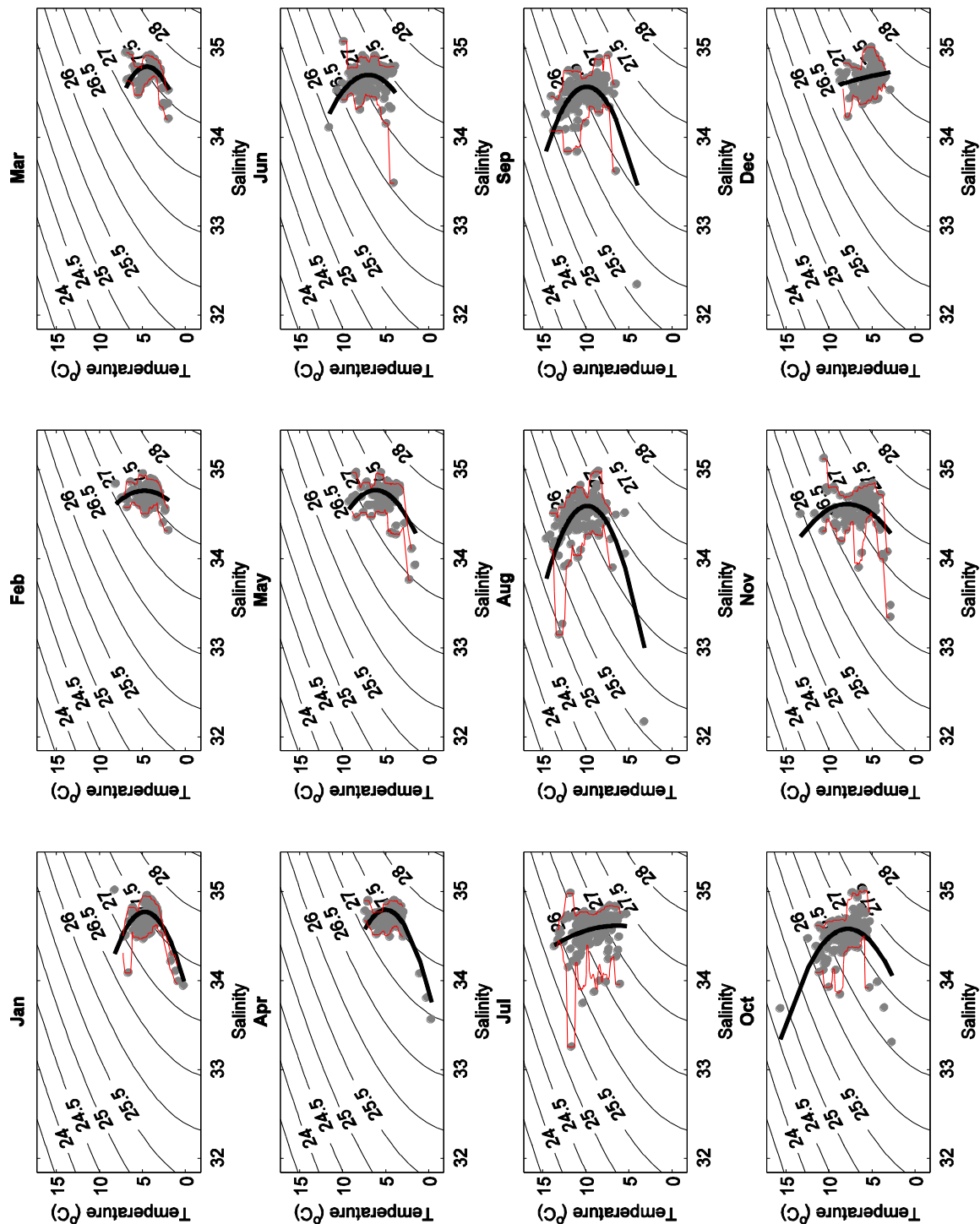


Figure 18 | East Basin Argo float shallower than 10m temperature and salinity monthly diagrams overlaid onto density contours. As figure 17, for the East Basin.

The next method of analyses was a single quadratic regression line to represent the monthly T-S relations across both regions (figures 17 and 18). A more straight forward approach than the first, a single quadratic regression has been applied to all Argo S measurements across all T values for each month at each region.

The quadratic curve noticeably represents the underlying ‘kinked’ winter T-S relationship within the West Basin well and eliminates the problem faced when using a piecewise linear regression of misalignment at the monthly mean T. This is particularly evident in summer months of both basins, where the quadratic curve represents T-S data well and remains within the upper and lower bounds considerably better. A point of interest is how the quadratic coefficients in the West Basin become negative in winter and spring months. For example in March and April regression coefficients follow a negative parabola whilst the remainder of monthly coefficients demonstrate a positive parabola. For all months demonstrating positive parabolas the curved quadratic appears to underestimate S at T extremities, whilst conversely the two months demonstrating negative coefficients appear to overestimate at T extremities.

Whilst this method appears to remain within the 90% data bounds substantially better than the previous piecewise linear approach, the problem has not been eliminated. Despite this method being a noticeable improvement, a more dataset specific approach of generating coefficients universally between months and regions is further required (Maes *et al*, 1999).

6.2.3 Mixed Effects Spline Regression

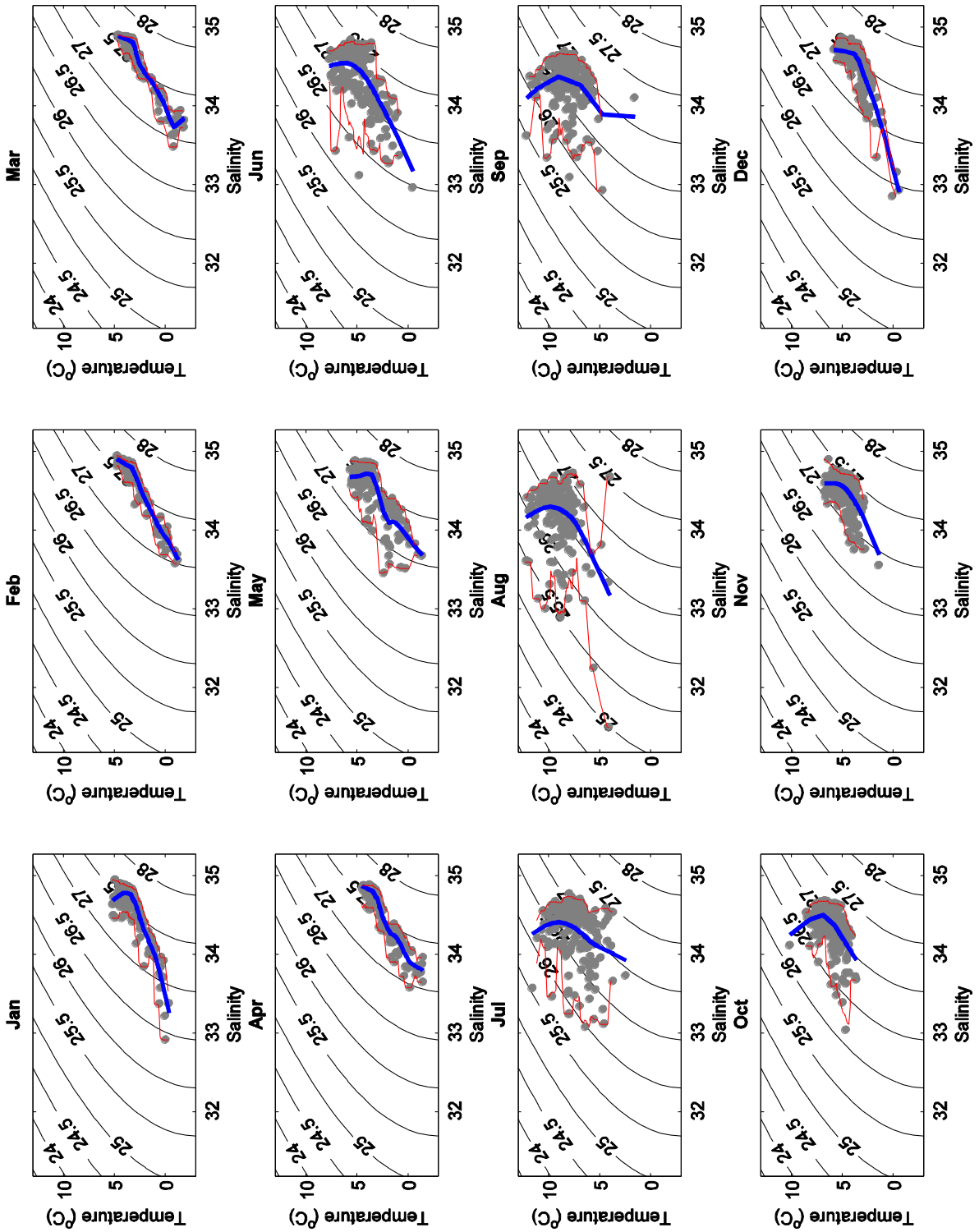


Figure 19 | West Basin Argo float shallower than 10m temperature and salinity monthly diagrams overlaid onto density contours. The two red lines illustrate the 5% and 95% percentiles and the blue lines illustrates a single mixed effect spline regression for each month.

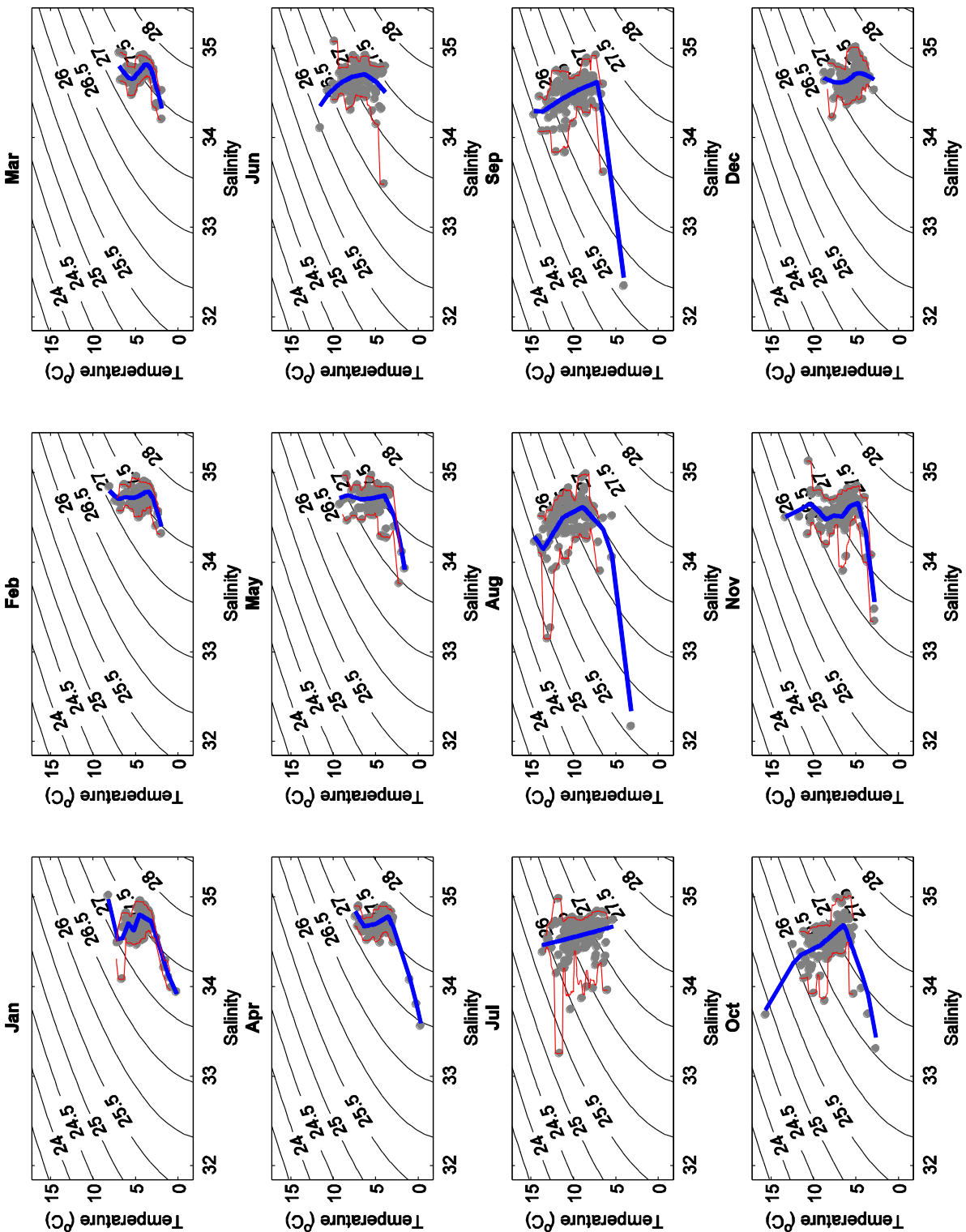


Figure 20 | East Basin Argo float shallower than 10m temperature and salinity monthly diagrams overlaid onto density contours. As figure 19, for the East Basin.

The final method analysed to represent T-S data more data specifically was a mixed-effect spline regression. Mixed effect models are a well-established method for providing flexibility when fitting models with various fixed and random elements. Recently mixed effect models have been combined with smoothing spline models, known for their flexibility in fitting a mean function onto arbitrary index sets to combine the power of smoothing to various fixed and random elements.

In a functional mixed effect model, the observations on subject i are assumed to have come from an underlying smooth function of time $y_i(t)$, which is decomposed into the following components:

$$\text{Equation 1: (Monique et al, 2005)} \quad y_i(t) = \mu(t) + v_i(t) + \varepsilon_i(t)$$

Where $\mu(t)$ is the mean function across all subjects, essentially treated as a fixed but unknown population parameter. $v_i(t)$ is subject i 's deviation from that mean function assumed to be randomly sampled from the population as a whole and $\varepsilon_i(t)$ is an error process.

To estimate the function $\mu(t)$ and the distribution of the functions $v_i(t)$, piecewise polynomial splines have been used. Essentially the piece polynomials control the smoothness or the non-linearity of the functions. Achieving the right level of smoothness is a critical aspect of the modelling process, too much smoothing and the underlying temporal dynamics will be lost; too little smoothing and spurious conclusions are likely to be made (Wang *et al*, 1998). To control the smoothness of a spline ‘knots’ are used to vary the number and location of breaks between polynomial pieces. For each monthly S dataset the minimum number of knots have been used that allow data gaps in S to be bridged by the spline regression (figures 19 and 20). Knot number is noted to vary for each T-S diagram as the spread of S with T differs between months and region. Between knots each polynomial (between specific T intervals) produces unique coefficients specific to the analysed T-S data and noise in S about this trend. It is important to note knots are distributed between maximum and minimum T values, meaning months with a higher T range (December - April) contain less measurements within each polynomial piece than low T ranging months (June - November) when the minimal threshold for knots is applied.

The use of minimal knots appears to avoid both spurious conclusions and over sampling of monthly T-S data to represent individual T-S relations well (figures 19 and 20). The polynomial pieces additionally appear to follow similar trends to the upper and lower bounds as well as being better confined to S values within them than previous methods, but does not eliminate the problem.

7 Evaluating Regression Choice

7.1 Temperature Averaged Salinity Residuals

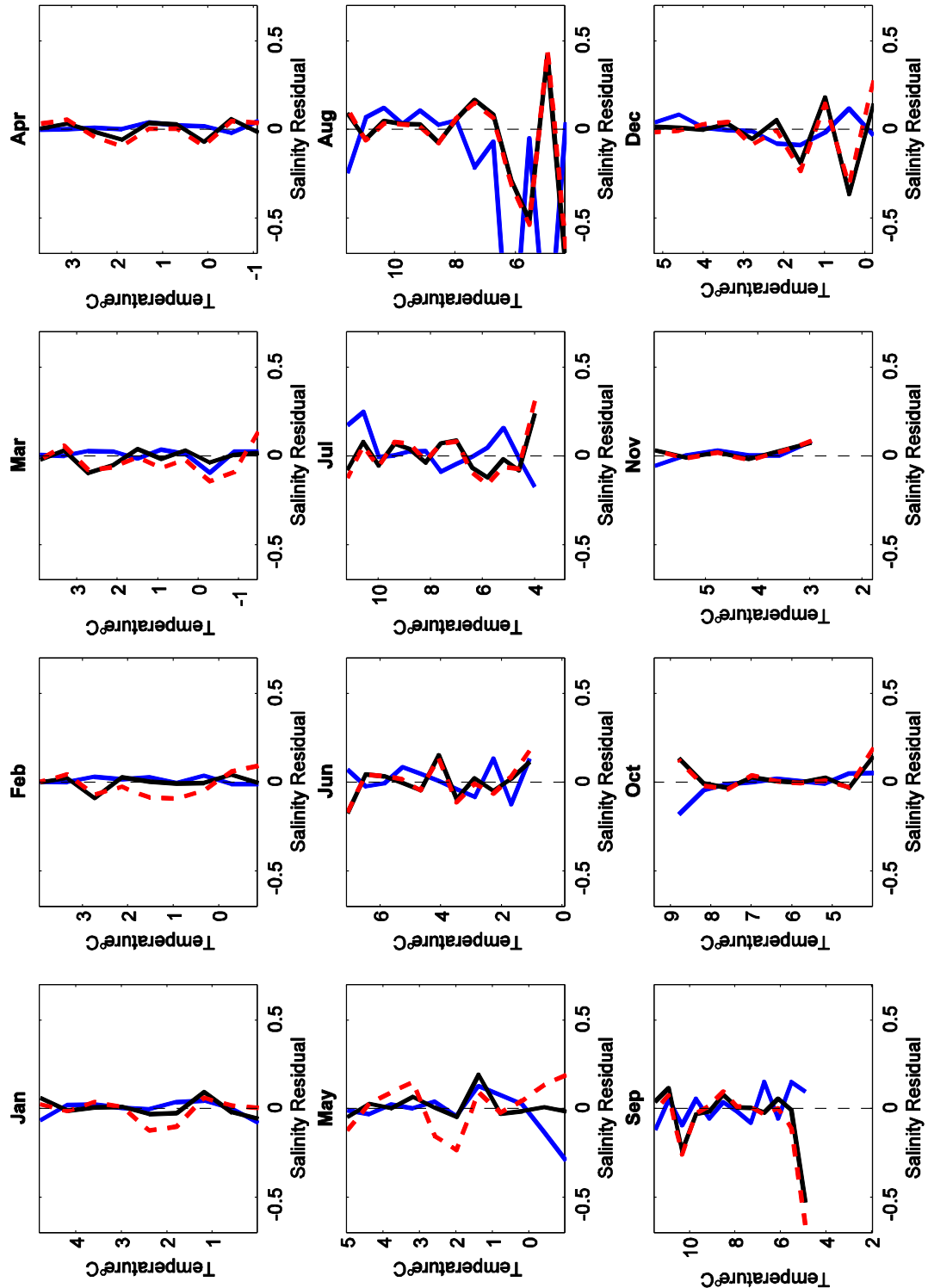


Figure 21 | West Basin Argo float salinity shallower than 10m vs salinity residuals of each regression method. The salinity residuals have been analysed across temperature intervals of 0.5°C . The blue lines illustrate the monthly piecewise linear residuals, the dashed red lines the quadratic residuals and black lines the mixed effect spline residuals.

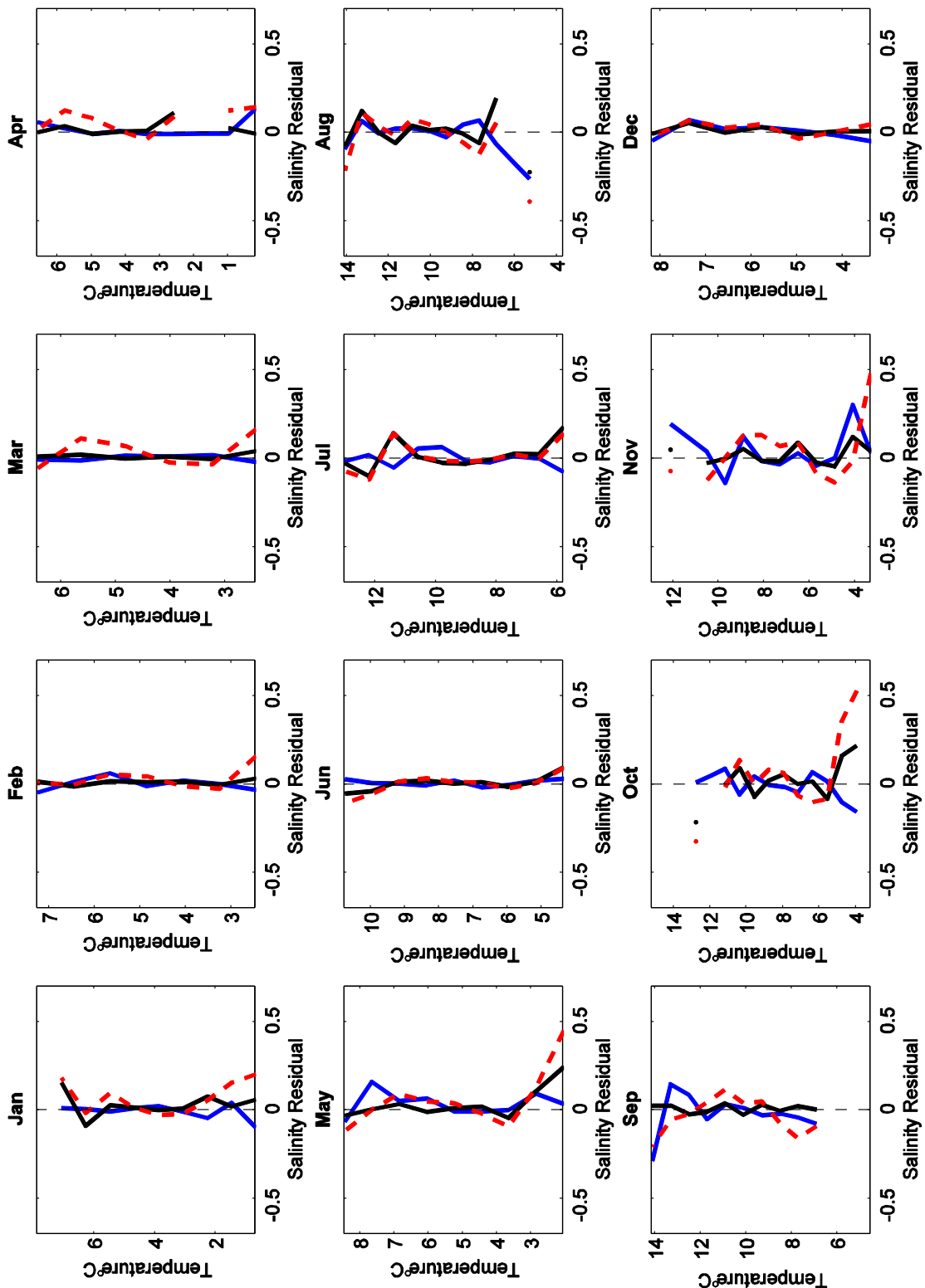


Figure 22 / East Basin Argo float salinity shallower than 10m vs salinity residuals of each regression method. As figure 21, for the East Basin.

Of the three methods analysed in section 6.2 the mixed effect spline regression appears to represent underlying Argo T-S relations best and this impression will be analysed more quantitatively in this section. The S residuals, calculated by subtracting observed Argo S measurements from estimated regression values, have been averaged across 0.5°C T bins to show deviation trends in true values from predicted values.

The mixed effect spline regression deviates least from residual values of zero, implying the method represents Argo S measurements more accurately (figures 21 and 22). The residuals of the quadratic regression noticeably follow the mixed effect spline closely in summer months of both regions, although at T extremities the residuals deviate away from zero to higher values. In winter months both the piecewise linear and spline residuals remain close to zero across all T values, whilst the quadratic deviates considerably to higher residuals.

In summer months the piecewise linear approach changes from positive to negative residuals at the monthly mean T value as a result of a mismatch between linear regressions. The quadratic and spline residuals comparatively disagree more in summer months than winter months as expected, particularly in the West Basin. The greatest residual deviation to -0.74 occurs in the West Basin in August at a low T values of 1.5 °C. The East Basin illustrates a moderated winter to summer difference when compared to the strong error differences in the West Basin.

7.2 Temperature Averaged Salinity Root Mean Squared

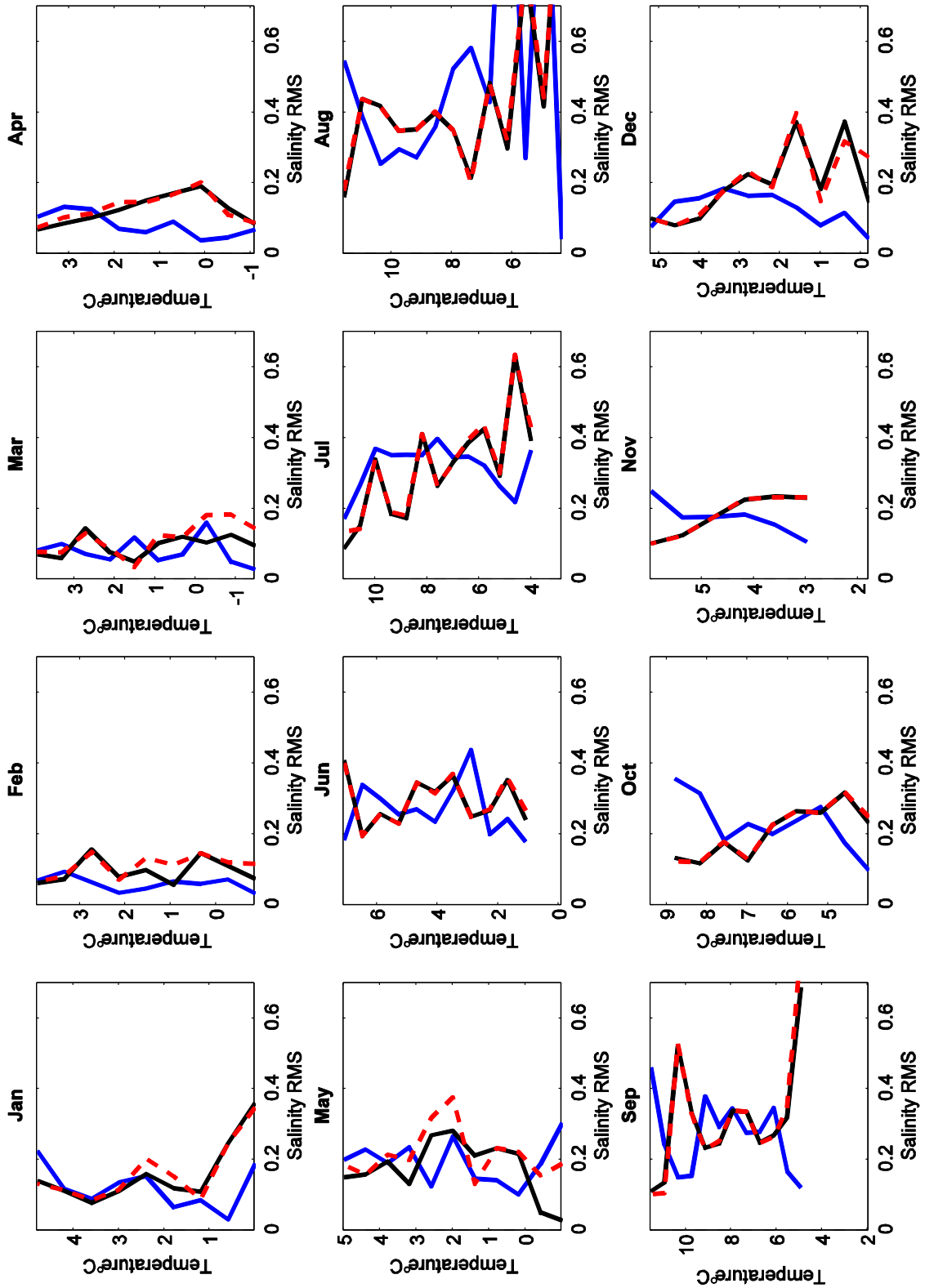


Figure 23| West Basin Argo float salinity shallower than 10m vs salinity root mean squared (RMS) of each method. The salinity residuals have been analysed across temperature intervals of 0.5°C . The blue lines illustrate the monthly double linear residuals, the dashed red lines the quadratic residuals and black lines the mixed effect spline residuals.

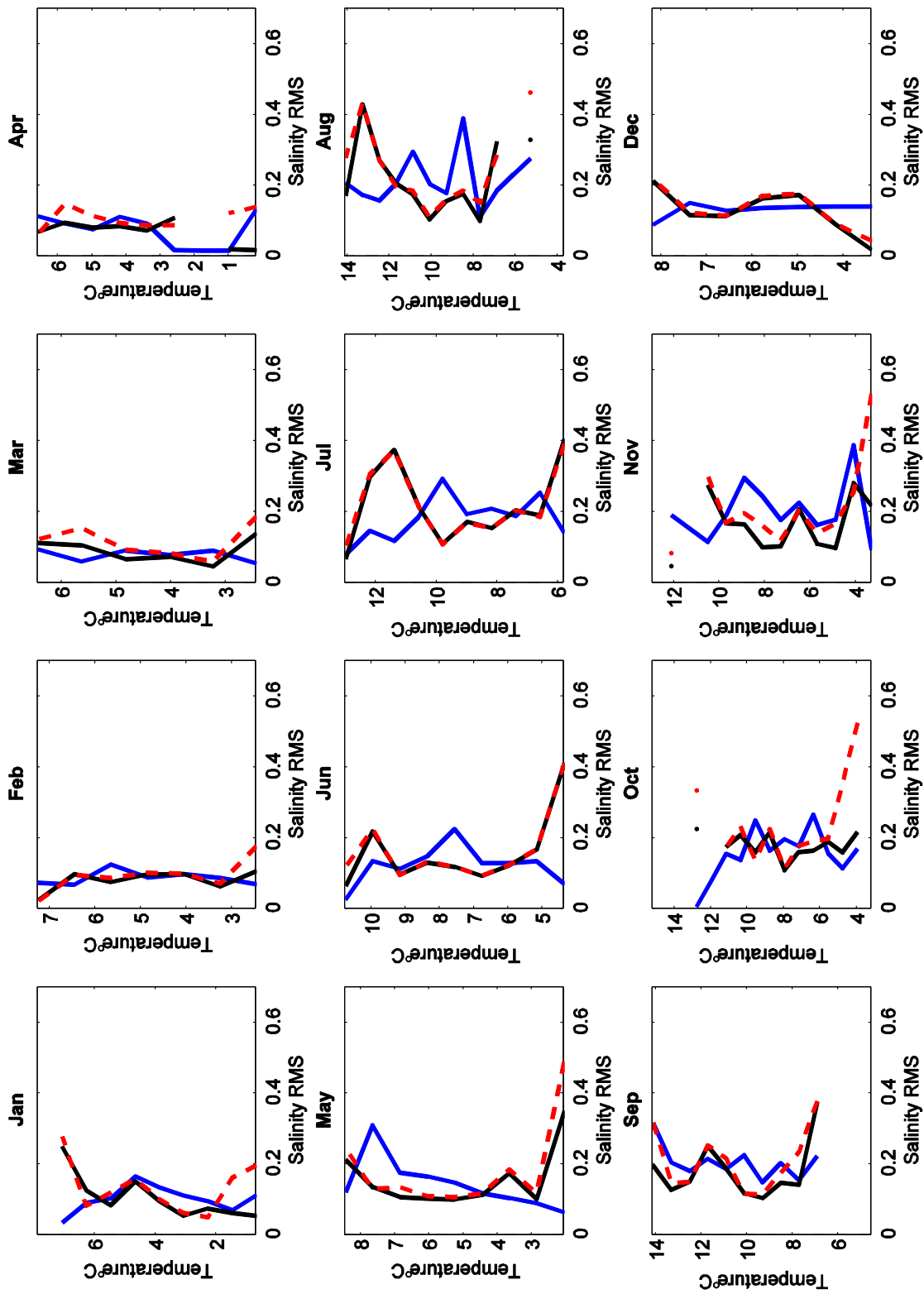


Figure 24 | East Basin Argo float salinity shallower than 10m vs salinity root mean squared (RMS) of each method. As figure 25, for the East Basin.

Another method for analysing which regression method best fits underlying T-S data is the Root Mean Squared (RMS), a meaningful measure of the error (figures 23 and 24). The RMS of the observed and predicted difference serves as an accurate measure for how far on average the error is from zero. Similarly to calculated residuals, deviation trends in RMS values have been shown by averaging across 0.5°C T bins.

The RMS values highlight overall residual deviations regardless of being positive or negative. Figures 23 and 24, much like figures 21 and 22, indicate that the West Basin has larger associated errors than the East. However, whilst the spline regression in the West Basin is expected to be the closest to S RMS values of zero the linear approach appears across most months as good a fit. The quadratic and spline RMS values once again are similar to one another but at extreme T values the spline approach maintains lower RMS values. In the summer months the spline and quadratic are substantially better than the piecewise linear regression for both the East and West Basin, agreeing with initial results from section 6.2.

In summary, residual and RMS analysis agrees with initial findings of the mixed effect spline regression being the best method for representing monthly Argo float S measurements in both the East and West Basin. As a result of better agreement with 5% and 95% bounds, less deviation of predicted values from true values and better adaptability to monthly T-S relations the mixed effect spline regression has been used in further SSS reconstruction.

8 SSS Reconstructions

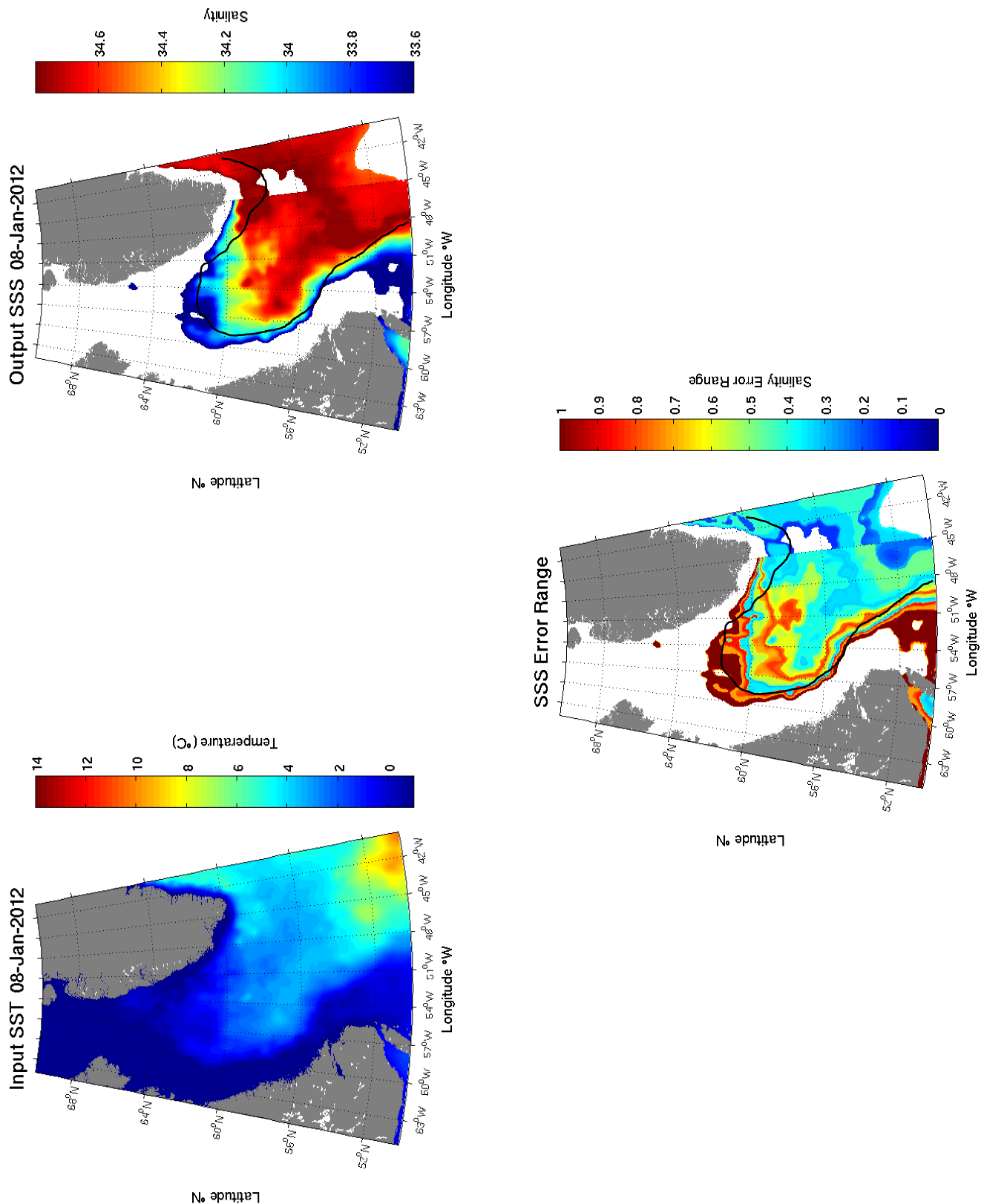


Figure 25/ 8th January 2012 OSTIA SST, Reconstructed SSS and associated SSS error ranges. The upper left figure shows the Input OSTIA SST from 08 January 2012 and the upper right the output reconstructed SSS OSTIA SSS based on monthly mixed effect spline regressions. Waters deeper than the 2000m isobar line in black indicates where reliable predictions are considered to occur. The lower figure shows the SSS Error Range, calculated by taking away the upper SSS limit from the lower SSS limit output by the function.

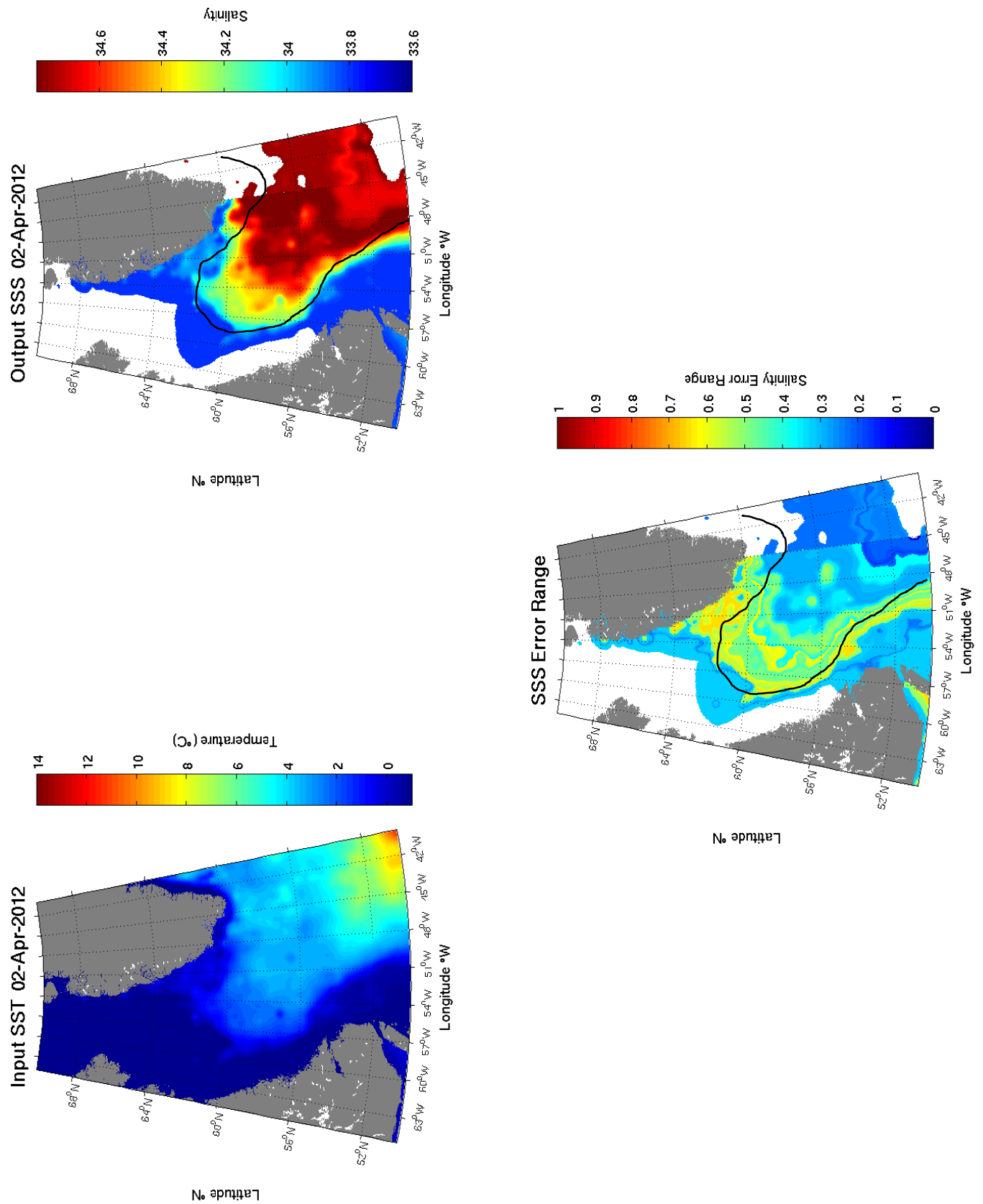


Figure 26/ 2nd April 2012 OSTIA SST, Reconstructed SSS and associated SSS error ranges. As figure 25, for the 2nd April 2012.

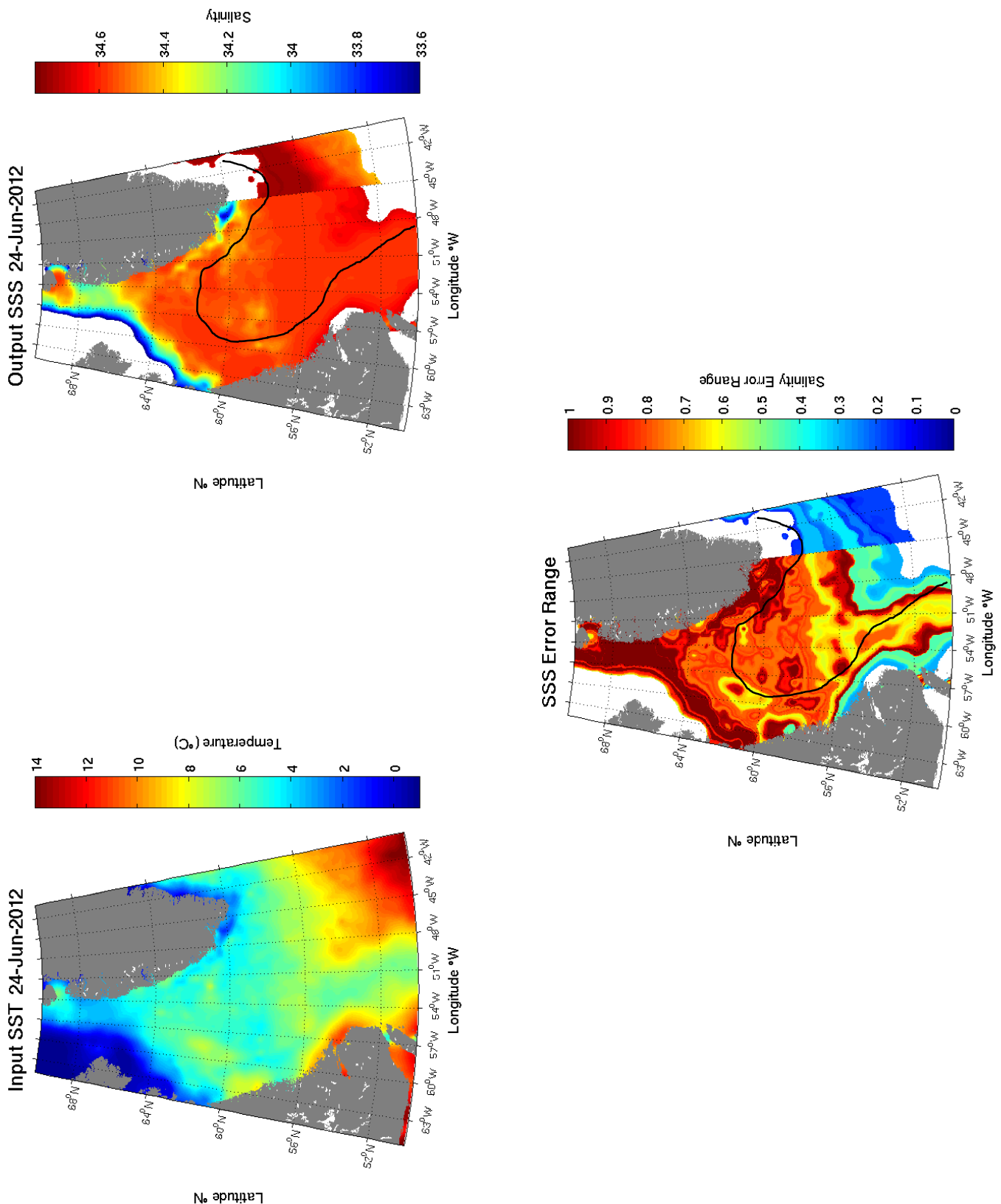


Figure 27| 24th June 2012 OSTIA SST, Reconstructed SSS and associated SSS error ranges. As figure 25 and 26, for the 24th June 2012.

Further analysis of reconstructed SSS within this study uses OSTIA data, shown in section 5 to be strongly correlated to Argo float measurements collected shallower than 10m. The aim is to express SSS as a function of a number of variables: SST, latitude, longitude and time within a Matlab function. The Matlab function additionally requires the input of a predetermined Matlab file containing the error bounds and coefficients calculated using the mixed effect spline regressions in chapter 6.1.

Reconstructed SSS from January, April and June 2012 and the associated range in SSS error are shown in figures 25, 26 and 27. Based on the T-S diagrams for January and April both the East and West Basins demonstrated a strong T-S relation and are well represented by the mixed effect splines. Consequently January and April can be regarded to reconstruct SSS well and demonstrate small SSS error ranges (between 1.1 and 0.25, and 0.6 and 0.14, respectively). The non-normal data distribution and deviation of regression lines from central values means the error bars cannot be implied as a \pm error. However, plotting the upper and lower bounds as an error range aids the identification of where high and low uncertainties occur. Moreover, SSS estimations in waters shallower than 2000m are considered to have substantial uncertainties associated with them. This is due to the T-S relations in this study used for reconstruction being based on interior waters deeper than 2000m. From the limited shelf sea Argo float measurements available (figure 6) it is reasonable to assume shelf waters fluctuate in T and S considerably more and demonstrate different T-S relations than basin waters analysed. Additionally, in SSS reconstructions data gaps (evident in figures 25, 26 and 27) are created by input SST values being outside of the Argo float T range (12.7 to -1.9°C). As a result SSS is not computed for these measurements to prevent extrapolation of results to inaccurate S values.

Between December and May waters deeper than 2000m SSS are regarded to be well reconstructed. In contrast, from June to November, where T-S relations appear to breakdown, the spatial reconstructions are incoherent between months. Video 1 (a video showing input OSTIA SST, reconstructed SSS and the SSS error range through 2012 at 2 day temporal resolution) indicates the reconstructed SSS for these months contrast one another considerably, resulting in an apparent ‘flashing’ of the video. This could possibly be due to quick T changes associated with atmospheric heating and cooling the surface ocean (Giglio *et al*, 2014). Conversely, between December and May a good coherence in SSS values exists between months, outlined by January and May showing a similar range in SSS values within the Basin (~34.8 - 33.9 and ~34.9 - 34.1, respectively). It is important to mention that associated S error ranges in reconstructed SSS are similar or lower than seasonal S

ranges observed to occur in the basin (figure 8 and table 1 of ~ 0.6 and 0.9 for the East and West Basin, respectively).

From December-May high S values occur in deeper waters whilst low S values are present in shallower waters and vice versa for T. Around continental shelves where boundary currents occur the greatest horizontal S gradients are visible, this front between low and high S values appears to migrate from shallow waters in winter months to deeper waters in summer months. This occurs at intermediate SSS values reconstructed close to continental shelf waters, where the largest error ranges are visible (~ 1.1 and 0.6 for figures 25 and 26, respectively). Interestingly from the SSS error ranges for January and April what appear to be identifiable as boundary currents are associated with the largest errors, implying such currents are associated with large uncertainties in T-S relations.

Between June and November the breakdown in T-S relations means mixed effect spline regressions represent S across all T values relatively poorly. When SST is shown to be reasonably uniform across the majority of the Labrador Sea, reconstructed SSS is estimated to be coherently high. Earlier T-S diagram analysis indicates a wide range of S values occur across all T values over summer months, meaning these reconstructed values have a large associated error range of up to ~ 1.2 within the deep basin.

Compared to the West Basin, East Basin SSS reconstructions range in SSS substantially less seasonally and importantly appear coherent with SSS reconstructions west of 45°W in January and April. However in June the East and West Basins appear less coherent and vary in SSS by ~ 0.5 . Based on the lower SSS error range of ~ 0.2 seen in the East Basin it can be suggested the West Basin most likely underestimates S close to the East-West divide. Associated SSS error ranges are considerably less in the East basin than the West Basin, due to smaller variability in both T and S within the East basin.

An exciting prospect, apparent in SSS reconstructions from January and April 2012 are the suggestions of deep convection events around $\sim 57^{\circ}\text{N } 55^{\circ}\text{W}$. Around this location in January a patch of high S and low T is evident (~ 34.7 and $\sim -1.1^{\circ}\text{C}$, respectively). In April this circular zone becomes present once again, although demonstrates a low S value (~ 34.2) and a low T value ($\sim 0.5^{\circ}\text{C}$).

9 SSS Reconstructions Compared to Aquarius

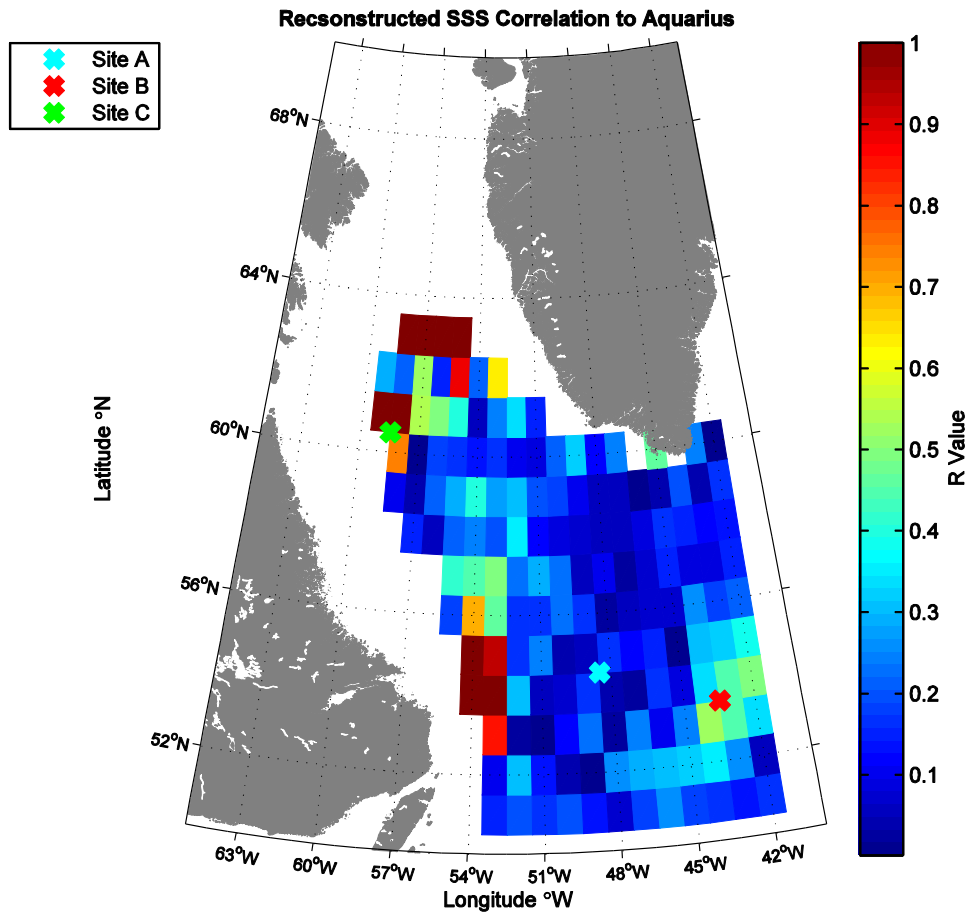


Figure 28| Reconstructed OSTIA SSS correlation to Aquarius SSS over winter months (December, January, February and March) between December 2011 and March 2014. Sites A, B and C illustrate the locations of time series analysed in figure 29.

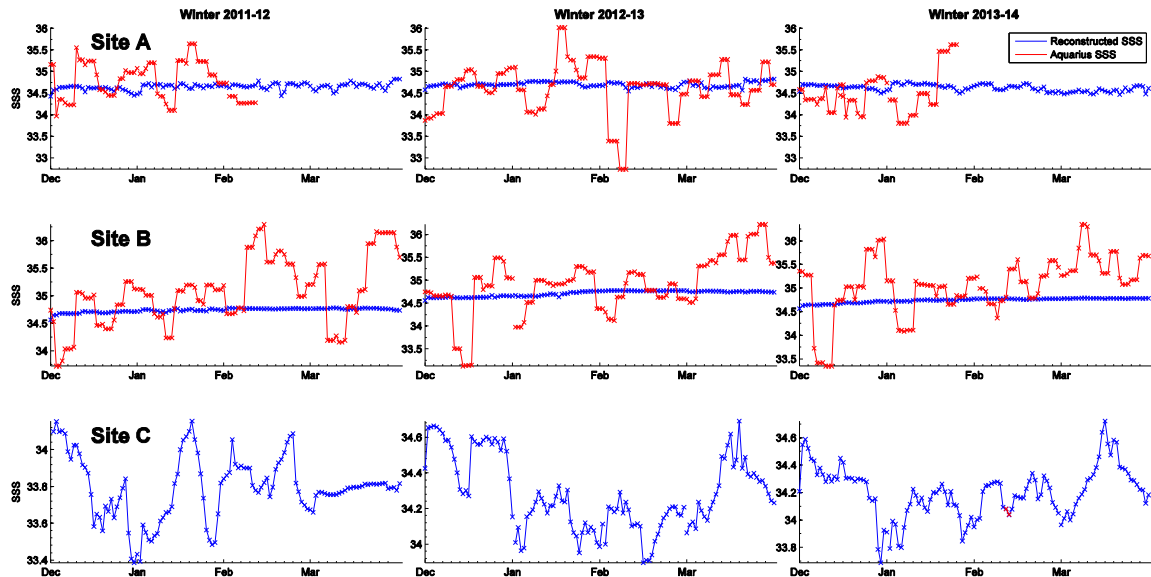


Figure 29| Time series of reconstructed OSTIA SSS (blue) and Aquarius SSS (red) across three winters 2011-12, 2012-13 and 2013-14 from sites A, B and C in figure 28.

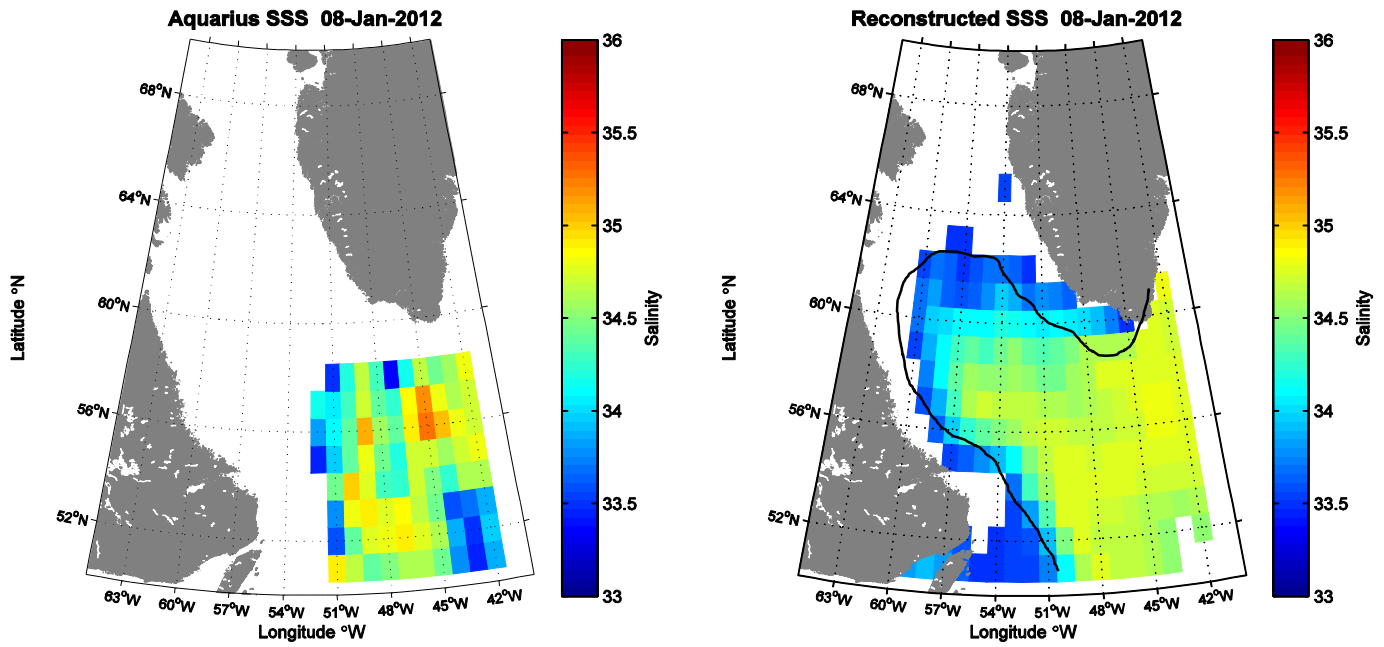


Figure 30| 8th January 2012 Aquarius 100km resolution SSS and reconstructed bin averaged 100km resolution SSS. Used to produce r values of correlation in figure 28.

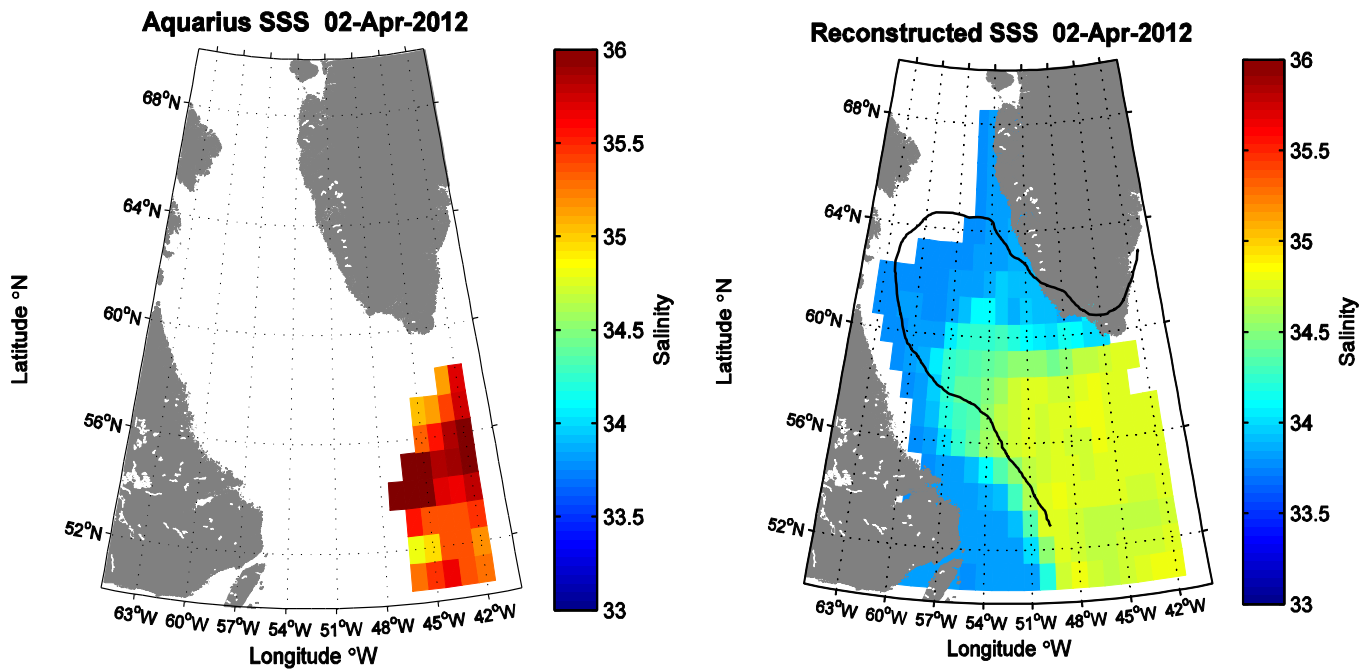


Figure 31| 2nd April 2012 Aquarius 100km resolution SSS and reconstructed bin averaged 100km resolution SSS, as shown in figure 30.

The next logical step is to compare reconstructed SSS calculated from OSTIA SST data to readily available level 3 Aquarius Data. The r value for Aquarius data and reconstructed SSS over winter months across a 3 year period (2011 to 2014) are shown in figure 28. This was achieved by bin averaging reconstructed SSS from a fine ~5km grid to match Aquarius's coarse 100km grid (figures 30 and 31).

Despite the mean r value between the datasets being ~0.47, a substantial region of the Labrador Sea illustrates low correlation between Aquarius and reconstructed SSS (r value of ~0.1), particularly between ~52°W and ~44°W. A time series at site 1 identifies this correlation is based on numerous winter measurements and supports the datasets being noticeably different (figure 29). The Aquarius SSS measurements vary considerably, fluctuating between 36.0 - 32.8 over the winters of 2011-12, 2012-13 and 2013-14, whilst reconstructed SSS measurements are markedly less variable (only fluctuating between 35 - 34.5). However, the mean S values of 34.7 and 34.6 for Aquarius and reconstructed SSS measurements, respectively suggest an underlying similarity exists. East of 45°W where minimal S variability occurs in Argo data a region of significant correlation is evident (r values of ~ 0.57). Importantly, the time series at site 2 (within this region) further highlights this correlation is based on a substantial number of Aquarius measurements (figure 29). Whilst Aquarius SSS is more variable than reconstructed SSS measurements an underlying similarity exists and agrees well at numerous times (e.g. at the middle to end of February 2013).

Finally the time series at site 3, where a significant relationship exists in the Western Labrador basin (r values from 0.55 to 0.95), indicates this high correlation is only based on a handful of Aquarius measurements, making them difficult to interpret. Although, of the two consecutive measurements available the datasets agree well.

Analysis of reconstructed SSS data against Aquarius measurements from January and April 2012 (figures 30 and 31) indicates Aquarius data is considerably more 'patchy' with larger SSS differences between 100km grids than bin averaged reconstructed SSS. Additionally, bin averaged SSS appears to underestimate SSS when compared to Aquarius measurements, resulting in large scale features such as differences between the shelf and deep basin appearing to be lost.

10 Discussion

The vertical structure of the water column is the result of an on-going competition between buoyancy inputs (solar heating and freshwater input) and mixing by tides in shallow waters (bottom up) and wind stress (top down). From the winter solstice to the vernal equinox the surface ocean experiences reduced solar and freshwater inputs of buoyancy, which act to stabilise the water column (Moore *et al*, 2003). As a result of reduced buoyancy the combination of mixing by tides and wind stress act to maintain a well-mixed water column. Within the deep Labrador Sea Basin wind stress is the predominant factor acting to mix the upper water column T and S down to the permanent pycnocline at ~1000m (Van Aken *et al*, 2011). From the vernal equinox the Labrador Sea experiences increased inputs of positive buoyancy via solar heating. Heating from the surface downward sets up bottom and top mixed layers, separated by a strong pycnocline that develops at a depth where the intensities generated by the two opposing forces are equal. Freshwater input to the Labrador Sea interior has been suggested to occur between spring–summer in two separate events; between April - May and July - September (Levitus *et al*, 2000; Schmidt and Send, *et al* 2007). The inflow of low S water overflows higher S ocean waters, inputting positive buoyancy from the surface down and further aiding stratification. The addition of wind stress can additionally enhance top down mixing of the surface warm-fresh layer to further depths.

Whilst Argo float measurements down to 10m are shown to be significantly correlated (~0.92) to OSTIA SST data the majority of spread originates from summer months when surface stratification occurs (figure 3). A substantial number of these points appear to occur in June when stratification begins to take hold of the upper few meters of the water column, suggesting Argo float measurements between the surface and 10m most likely sample either side of the pycnocline boundary. By September the height of stratification is achieved and minimal scatter about the linear trend is evident, implying Argo float measurements at 10m are within the upper well-mixed partition above the pycnocline. Unfortunately the requirement of a large dataset for T-S relation building means further removal of these values would reduce and not improve the accuracy of the regression. The future availability of a larger Argo float array within the Labrador Sea may allow for such a methods to be performed at a future date. The monthly breakdown of T and S is important as it highlights the scatter occurs over summer months, and a seasonal cycle exists between T and S where they appear linked in winter and unlinked in summer. Between June and November quick T changes associated with atmospheric heating and cooling may be the driving factor in T and S relations becoming broken (Ivchenko *et al*, 2010; Willis *et al*, 2004). As a result T and

S are most likely driven by differing processes when positive buoyancy is input to the surface ocean. Conversely, in winter and spring months when no net buoyancy is added to the ocean and mixing is solely present, T and S properties appear unaffected by rapid heating and cooling, although without analysing SST and SSS against ocean-atmosphere heat fluxes it is difficult to draw such conclusions.

Schmidt and Send, (2007) compared the timing and volume of seasonal freshwater influences to the Labrador Sea to conclude interior freshwater does not originate from local sources but instead externally from boundary currents. The origin of the first smaller pulse in April to May remains unclear but the second July to September pulse, about three times stronger and supplying ~60% of the seasonal summer freshwater, is suggested to originate from the West Greenland Current. Over summer months the external input of freshwater from afar alters the T-S relation, as low S measurements in the internal Labrador Sea are rarely low in T. A study by Hakkinen (2002) states large influxes of fresh water to the Labrador Sea occur in stages, influencing the shelf seas round June-July and eventually the basin by August-September.

Eddy kinetic energy at the North East tip of the Labrador Basin has been stated to correlate to deep convection and SSS within the internal Basin, implying eddies are important at transferring freshwater from boundary currents to the central basin and site of deep convection (Zhu *et al*, 2013). An inter-annual correlation has been suggested to additionally exist between Labrador Sea surface S and freshwater sources in the West Greenland Current and further upstream in the East Greenland Current, implying deep convection within the Labrador Sea is modulated by Arctic freshwater outflow (Schmidt and Send, 2007).

The late winter convection in the central Labrador Sea is strongly influenced by the prevailing stratification in late summer. For this late summer stratification S is as important as T, and in the upper water layers S even dominates. A key signature of open ocean deep convection are ‘chimneys’, which exist as ‘columns’ of mixed water observed to approach 100km in diameter and can reach down to the ocean floor under intense cooling of the sea surface (Helen, 2009; Robson *et al*, 2014). Such a chimney appears identifiable in figure 25 as a patch of high S and relatively low T around ~57°N 55°W. The high S suggests surface buoyancy within the local area has reduced beyond a critical level to allow homogenisation to be obtained between the surface and depth (Robson *et al*, 2014). This phase of ‘violent mixing’ exposes high S and low T by shoaling the pycnocline to surface depths. The well-defined near linear T-S relation over winter and spring may mean a T-S reconstruction model

can accurately identify S signals of deep convection with minimal error when the pycnocline shoals significantly.

Although OSTIA reconstructed winter SSS between 2011 and 2014 illustrates a low correlation to Aquarius SSS this could be due to a number of factors. Whilst bin averaging reduces the impact of read noise on the processed image, the approach removes sharp S gradients between pixels and blends the dataset together (Fryzlewicz and Van Keilegom 1998; Zhang *et al*, 2006). In contrast the 100km distance between Aquarius measurements illustrate sharp differences in S values between pixels. An alternative approach to better compare these two datasets may be to compute SSS from a 100km resolution microwave derived SST dataset and gain a similar S pixel contrast. The unsatisfactory resolution of Aquarius data in the Labrador Sea makes it increasingly difficult to draw conclusions from r values in figure 28. Importantly, maximum reconstructed SSS error ranges of ~1.3 computed for winter months are not greater than Aquarius errors of $\sim\pm 1$ and overlap estimated SSS values reconstructed in this study.

Further still, complex algorithm corrections to depict SSS signals from emitted long wave radiation are possibly a more complicated approach of measuring S, affected by more factors than the estimation of S from T. Currently no corrections are applied for the atmospheric contribution of liquid clouds and rain in SMOS and Aquarius data due to no simultaneous measurements of necessary parameters being on-board (Boyer *et al*, 2005). Very little is further known about the impact of rain on measured long wave radiation, although it is thought to have a dampening effect upon certain emitted wavelengths (Boutin *et al*, 2013).

As a consequence, these factors make it increasingly difficult to rule reconstructed SSS values as being completely inaccurate. Underlying similarities between Aquarius and reconstructed SSS values have been shown and the main differences appear to be the smaller variability in reconstructed values. Further analysis is undoubtedly required between better SSS datasets, although these are currently scarce and do not exist on useful timescales.

10.1 Limitations

The main difficulty faced when trying to obtain S estimations for the Labrador Sea is the lack of Argo float T and S observations to generate reliable and timely T-S relations, particularly in shelf seas. A limitation, specific to Argo floats, is that sensors are disabled at depths shallower than ~5m to prevent contamination from surfactants when sensors break the surface and to maintain long-term sensor calibration stability (Argo, 2011;

Lagerloef *et al*, 2011). Consequently, use of Argo data to represent SST and SSS may bring about biases when there are significant vertical gradient differences near the surface in summer months (as shown in figures 10 and 11) or input zones of heavy precipitation and freshwater (Lagerloef *et al*, 2011). No pumping has been shown to generate relatively inaccurate S values above ~5m. Comparisons performed in surface layers of a well-mixed area in the North Pacific between pumped and non-pumped Argo float S values indicated a noise associated with non-pumped S (at ~2m from the last pumped measurement) of 0.025 with respect to 0.005 of pumped S values (Boutin *et al*, 2013). It is additionally difficult to avoid the difference in Argo float ‘surface’ data and satellite 1mm “surface” data, but the two data sets are shown to be relatively well correlated and the 0.0005°C and 0.01 accuracy of Argo float T and S measurements respectively is seen to outweigh this limitation (Argo, 2011).

Another limitation to consider is error propagation from SST data used to reconstruct SSS. The use of infrared satellite SST, which has the benefit of high spatial and temporal resolution is susceptible to cloud contamination and data gaps (Reynolds *et al*, 2002). Based on this, high precision level 4 composite data, such as OSTIA SST used in this study, is advised as an input SST to minimise further errors (Donlon *et al*, 2008). Reconstructed SSS is limited to observed ranges in Argo float T and S, to prevent extrapolation beyond observed values. When OSTIA SST data is input figures 25, 26 and 27 highlight considerable data gaps occur as a result of SST values being outside of observed Argo float T measurements between 2002 and 2012. This raises the question of the datasets measuring different T values in the same location and over the same time period. However Argo float measurements cover only a single location in time within the Labrador Basin, compared to satellite SST datasets, which cover a large area in a single time step. Reduction of data gaps is therefore only achievable with increased Argo float coverage. One of the main drawbacks of the T-S relation module is the quantification of errors from the regression estimate. Whilst the use of percentiles illustrates where the majority of data exists within the non-normally distributed datasets it is a relatively crude approach and severely restricted by the number of Argo data points present. Despite the mixed effect model representing Argo T-S data best of the analysed methods, the problem of regression lines estimating values outside of the upper and lower bounds is an issue that has only been minimised.

10.2 Potential Application

The potential applications of such a SSS lookup map are broad. The knowledge of SSS could be used for reconstruction of vertical density or velocity fields from well-developed vertical T-S models that require SSS for improved accuracy (Han *et al*, 2004; Thacker *et al*, 2007; Vossepoel *et al*, 1999). Moreover, due to the winter stability of the Labrador interior basin reconstructed SSS could be useful to validate remotely sensed S missions (such as SMOS or Aquarius). Additionally, higher resolution SSS maps than currently available 100km satellite observations could be derived from high resolution SST, Argo-float or Glider SST datasets. Initial findings from this study suggest deep convection could additionally be monitored, as sinking water punctures the pycnocline exposing deep saline water to detectable surface depths. This provides supplementary data into research about freshwater inputs, such as hosing events, on deep convection and subsequently the AMOC.

11 Conclusion

11.1 Summary of Results

The results from this paper aimed to identify whether an S look up table could be constructed from T in the Labrador Sea. The use of high precision Argo float T measurements up to 10m depth have shown to be significantly correlated to level 4 OSTIA SST ($r = 0.912$). A strong seasonal variability in Argo float T-S relations are shown to exist within the Labrador Basin, where winter and spring months illustrate a confined nearly linear relation, ideal for estimating S from T. T-S diagrams of summer and autumn months on the other hand are considerably scattered as a result of relations ‘breaking down’, making it difficult to reconstruct S accurately. The method deemed to represent individual monthly T and S data best, based on the smallest residuals, was the use of a mixed effect spline regression, a single method capable of adapting to individual datasets. Other relatively simple regression lines appear unable to adapt to the relatively complex T-S relations shown to exist at different regions and times of year.

The ~5km high-resolution reconstructed OSTIA SSS illustrates the major S features within the Labrador Basin. Events within the West Basin, such as deep convection may be visible in SSS. Whilst summer months show large associated error ranges, winter months show low ranges. The strong correlation between Argo surface T and OSTIA SST, and the tight Argo T-S relationship in winter months suggest wintertime SSS reconstructions should be reasonably accurate. However, well correlated winter reconstructed SSS values only correlate

reasonably with Aquarius SSS in the East and West basin and poorly in the central basin, although further analysis and development is undoubtedly required.

11.2 Future Considerations

The inability to reconstruct shelf sea S will remain a caveat until Argo float coverage becomes more spatially and temporally consistent, or another data source is used. Additionally, other than simply allowing temporal variability to exist, further spatial separation than East and West Basin should be considered as numerous fluctuations in T and S remain present. In particular further separation of boundary currents from the West Basin would be beneficial as summer S values were shown to vary inter-annually due to their close proximity to boundary currents in some years. The influence of freshwater from boundary currents is known to differ locally and further separation may reduce summer scatter observed in the large West Basin region and consequently errors. Whether rapid atmospheric heating and cooling of the surface ocean is responsible for the breakdown in T-S relations requires further research. This study does not analyse the influence of surface heat fluxes on Argo T and S measurements to draw further conclusions on T-S relations breaking down.

11.3 Take Home Message

It is well accepted and documented that S can be estimated from T observations and Argo floats are powerful instruments for measuring these variables. The possibility of generating a high resolution SSS map for the Labrador Sea from SST data is an exciting prospect with many potential applications. Initial findings are positive, highlighting a significant T-S relation exists in winter months and provide a platform for future research. Whilst limitations with the method have been identified there is significant room for further development highlighted in this study, to reduce associated errors.

12 References

- Argo. Argo Float Data Accuracy. (2011). Available: <http://www.argo.ucsd.edu/FAQ.html>. Last accessed 29th May 2014.
- Ballabrera-Poy. J., Mourre. B., Garcia-Ladona. E., Turiel. A. and Font. J. (2009). Linear and non-linear T-S models for the eastern North Atlantic from Argo data: Role of surface salinity observations. *Deep-Sea Research I*. **56**, p.1605–1614.
- Belkin. I. M., Levitus. S., Antonov. J. and Malmberg. A. S. (1998) “Great Salinity Anomalies” in the North Atlantic. *Progress in Oceanography*. **41**, p.1-68.
- Boutin. J., Martin. N., Reverdin. G., Yin. X. and Gaillard. F. (2013). Sea surface freshening inferred from SMOS and ARGO salinity: impact of rain. *Ocean Science*. **9**, p.183-192, doi:10.5194/os9-183-2013.
- Bowen. M., Sutton. P., Roemmich. D. (2014) Estimating mean dynamic topography in boundary currents and the use of Argo trajectories. *Journal of Geophysical Research-Oceans*. **119**, p.8422-8437. doi: 10.1002/2014jc010281.
- Boyer. T. P., Levitus. S., Antonov. J. I., Locarnini. R. A and Garcia. H. E. (2005). Linear trends in salinity for the World Ocean, 1955-1998. *Geophysical Research Letters*, **32**, p.1-4, doi: 10.1029/2004GL021791.
- Broecker. W. S. (1991) The Ocean Conveyor. *Oceanography*. **4** (2). p.79-88.
- Dickson. R. R., Yashayaev. I., Meincke. J., Turrell. W., Dye. S. and Holfort. J. (2002) Rapid freshening of the deep North Atlantic Ocean over the past four decades. *Nature*, **416**, p.832-837.
- Donlon. C. J. (2006) The Global Ocean Data Assimilation Experiment High Resolution Sea Surface Temperature Pilot Project (GHRSST-PP) Data Processing Specification version 1.7 (GDSv1.7), *GODAE project*. p.270.
- Donlon. C. J., Robinson. I., Casey. K., Vasquez. J., Armstrong. E., Gentemann. C., May. D., LeBorgne. P., Piollé. P., Barton. I., Beggs. H., Poulter. D. J. S., Merchant. C., Bingham. A., Heinz. S., Harris. S., Wick. G., Emery. B., Stuart-Menteth. A., Minnett. P., Evans. B., Llewellyn-Jones. D., Mutlow. C., Reynolds. R., Kawamura. H. and Rayner. D. (2008) The Global Ocean Data Assimilation Project (GODAE) High Resolution Sea Surface Temperature Pilot Project (GHRSST-PP), *Bulletin of the American Meteorological Society*, **6**. p.341-350.
- Emery. W. J. (1975). Dynamic height from temperature profiles. *Journal of Physical Oceanography*. **5** (2), p.369–375
- Emery. W. J. and Wert. R. T. (1976). Temperature–salinity curves in the pacific and their application to dynamic height computation. *Journal of Physical Oceanography*. **6** (4), p.613–617.
- Emery. W. J., and Thomson. R. E (2001). Data Analysis Methods in Physical Oceanography. *London: Elsevier*. **2** (13), p.193-304.
- Fryzlewicz. P. and Van Keilegom. I. (1998). Series B (Statistical Methodology), ISSN 1467-9868, *Journal of the Royal Statistical Society*, **60** (1) p.159-174.
- Giglio. D. and Roemmich. D. (2014) Climatological monthly heat and freshwater flux estimates on a global scale from Argo. *Journal of Geophysical Research-Oceans*. **119**, p.6884-6899. doi: 10.1002/2014jc010083.
- Glessmer. M. J., Eldervik. T., Vage. K., Nilson. J. E. and Behrens. E. (2014) Atlantic origin of observed and modelled freshwater anomalies in the Nordic Sea. *Nature Geoscience*. **7**, p.801-805. doi:10.1038/ngeo2259.
- Haines. K. (2006) Salinity Assimilation using S9T: Covariance Relationships. *American Meteorological Society*. **72**, p.759-771.
- Hakkinen. S. (2002). Freshening of the Labrador Sea surface waters in the 1990s: Another great salinity anomaly? *Geophysical Research Letters*. **29** (24), p.85-89.
- Han. G. and Zhou. J. (2004). Salinity estimation using T-S relation in the context of variational data assimilation. *Journal of Geophysical Research*, **109**, p.1-12, doi: 10.1029/2003JC001781.
- Hansen. D.V. and Thacker. W.C. (1999). Estimation of salinity profiles in the upper ocean. *Journal of Geophysical Research*. **104** (C4), p.7921–7933.
- Helen. J. (2009) Open Ocean Deep Convection. Available: <http://puddle.mit.edu/~helen/oodc.html>. Last Accessed: 1st April 2015.
- Ivchenko. V. O., Wells. N. C. Aleynik. D. L. and Shaw. A. G. P. (2010) Variability of heat flux and salinity contention in the North Atlantic in the last decade. *Ocean Science*, **(6)**, p. 719-735. doi:10.5194/os-6-719-2010.

- Kleinen. T., Osborn. T. J. and Briffa. K. R. (2009). Sensitivity of climate response to variations in freshwater hosing location. *Ocean Dynamics*. **59** (1), p.509-521.
- Kummerow. C., Hong. Y., Olson. W. S., Yang. S., Adler. R. F., McCollum. J., Ferraro. R., Petty. G., Shin. D. B., Wilheit. T. T. (2010) The Evolution of the Goddard Profiling Algorithm (GPROF) for Rainfall Estimation from Passive Microwave Sensors. *Journal of Applied Meteorology* **40** (11), p.1801-1820.
- Lab Sea Group. (1998). The Labrador Sea deep convection experiment. *Bulletin of the American Meteorological Society*. **79**, p.2033–2058.
- Lagerloef. G., Boutin. J., Chao. Y., Delcroix. T., Font. J., Niiler. P., Reul. N., Riser. S., Schmitt. R., Stammer. D. and Wentz. F. (2011). Resolving the global surface salinity field and variations by blending satellite ad In-situ observations. *Journal of Climate*, **32**, p.34-56.
- Levitus. S., Antonov. J. I., Boyer. P. and Stephens. C. (2000). Warming of the World Ocean. *Science*, **287**. p2225-2229, doi: 10.1126/science.287.5461.2225.
- Maes. C. and Behringer. J. (1999). Why salinity variability must be considered more accurately by ocean GCM's? *Geophysical Research Abstract*, **1** (368), p.361-386.
- Marrero-Diaz. A., Rodriguez-Santana. A., Machin. F. and Pelegri. J.L. (2006). Analytic salinity–temperature relations for the upper-thermocline waters of the eastern North Atlantic subtropical gyre. *Scientia Marina*, **70** (2), p.167–175.
- Marshall. J. and Schott. F. (1999) Open Ocean Convection: Observations, theory and models. *Reviews of Geophysics*, **37** (1). p.1-64. doi: 10.1029/98RG02739.
- McGeehan. T. and Maslowski. W. (2011) Impact of Shelf–Basin Freshwater Transport on Deep Convection in the Western Labrador Sea. *Journal of Physical Oceanography*. **41** (11), p. 2187-2199. doi:<http://dx.doi.org/10.1175/JPO-D-11-011.1>.
- Meijers. A. J. S. and Bindoff. N. L. (2011). Estimating the Four-Dimensional Structure of the Southern Ocean Using Satellite Altimetry. *Journal of Atmospheric and Oceanic Technology*, **28** (17), p.548-568.
- Monique. L., Mackenzie. C. R., Donovan. B. H. and McArdle (2005) Regression Spline Mixed Effect Models: A forestry example. *Journal of Agricultural, Biological and Environmental Statistics*, **10** (4). p.394-410.
- Moore. C. M. (2003). Physical controls on phytoplankton physiology and production at a shelf sea front: a fast repetition-rate fluorometer based field study. *Marine Ecology - Progress Series*. 259, p.29-45,
- Reverdin. G., Cayan. D. and Kushnir. Y. (1997). Decadal variability of hydrography in the upper northern North Atlantic in 1948–1990. *Journal of Geophysical Research* **102**, p.148-151. : doi: [10.1029/96JC03943](https://doi.org/10.1029/96JC03943).
- Reynolds. R. W., Rayner. N. A., Smith. T. M., Stokes. D. C. and Wang. W. (2002) An improved in situ and satellite SST analysis for climate, *Journal of Climate Science*, **15**. p.1609–1625.
- Robson. J., Sutton. R. and Smith. R. (2014) Decadal predictions of the cooling and freshening of the North Atlantic in the 1960's and the role of the ocean circulation. *Climate Dynamics*. **42** (9), p.2353-2365. doi:[10.1007/s00382-014-2115-7](https://doi.org/10.1007/s00382-014-2115-7).
- Roemmich. D. (2009) Argo: the challenge of continuing 10 years of progress. *Oceanography*. **22**. p.46-55. doi: [10.5670/oceanog.2009.65](https://doi.org/10.5670/oceanog.2009.65).
- Roemmich. D., Johnson. G.C., Riser. S., Davis. R., Gilson. J., Owens W.B., Garzoli. S.L., Schmid. C. and Ignaszewski. M. (2009). The Argo Program: Observing the global ocean with profiling floats. *Oceanography* 22(2). p.34–43, doi.org/[10.5670/oceanog.2009.36](https://doi.org/10.5670/oceanog.2009.36).
- Schmidt. S. and Send. U. (2007) Origin and composition of seasonal Labrador Sea freshwater. *American Meteorological Society*, **37**, p.1445-1454.
- Solomon. S., Qin. D., Manning. M., Chen. Z., Marquis. M., Averyt. K. B., Tignor. M and Miller. H. L. (2007). IPCC Fourth Assessment Report Climate Change 2007: Working Group I: The Physical Science Basis. North Atlantic Subplot Gyre, Labrador Sea and Nordic Seas. p.785-967.
- SPURS. (2012). Why is it Important to Understand Ocean Salinity? Available: http://cosee.umaine.edu/coseeos/spurs/why_resources1.htm. Last accessed 26th Apr 2014.
- Stark. J. D., Donlon. C. J., Martin. J. M. and Colloch. M. E. (2007) OSTIA: An Operational, high resolution, real time, global sea surface temperature system. *Bulletin of the American Meteorological Society*. **3**, p.1-4.

- Sundby. S. and Drinkwater. K. (2007). On the mechanisms behind salinity anomaly signals of the northern North Atlantic. *Progress in Oceanography*, **73** (67), p190-202.
- Thacker. W. C. (2007). Estimating salinity to complement observed temperature in the Gulf of Mexico. *Journal of Marine Systems*, **65**, p.224-248.
- Van Aken. H. M., Jong. M. F. and Yashayaev. I. (2011) Decadal and multi-decadal variability of Labrador Sea Water in the north-western North Atlantic Ocean derived from tracer distributions: Heat budget, ventilation, and advection. *Deep Sea Research Part I: Oceanographic Research Papers*. **58** (5), p. 505-523. doi:10.1016/j.dsr.2011.02.008.
- Vossepoel. F.C., Reynolds. R.W. and Miller. L. (1999) Use of sea level observations estimate salinity variability the tropical Pacific. *Atmospheric Oceanography Technology*. **54**, p.1404-1414.
- Wang. Y. (1998). Mixed Effects smoothing spline analysis variance. *Journal of Royal Statistical Society*. **60** (1), p. 159-174.
- Willis. J. K., Roemmich. D. and Cornuelle. B. (2004). Inter-annual variability in the upper ocean heat content, temperature and thermometric expansion on global scales. *Journal of Geophysical Research*, **109**(C12036). p.1-13, doi:10.1029/2003JC002260.
- Zhang. X-P., Rehtanz. C. and Pal. B. C. (2006). Flexible AC Transmission systems: Modelling and Control, ISBN 3-540-30606-4, Monograph, *Springer Power Systems Series*, p.1-383.
- Zhu. J., Demirov. E. Zhang. Y. Polomska-Harlick. A. (2014) Model simulations of mesoscale eddies and deep convection in the Labrador Sea. *Advances in Atmospheric Science*. **31** (4), p.743-752. doi:10.1007/s00376-013-3107-y.